

Concentrations and radiative forcing of anthropogenic aerosols from 1750-2014
simulated with the OsloCTM3 and CEDS emission inventory

Marianne Tronstad Lund^{1*}, Gunnar Myhre¹, Amund Søvde Haslerud¹, Ragnhild Bieltvedt Skeie¹,
Jan Griesfeller², Stephen M. Platt³, Rajesh Kumar^{4,5}, Cathrine Lund Myhre³, Michael Schulz²

1 CICERO Center for International Climate Research, Oslo, Norway

2 Norwegian Meteorological Institute, Oslo, Norway

*3 NILU – Norsk institutt for luftforskning, Dept. Atmospheric and Climate Research (ATMOS),
Kjeller, Norway*

4 Advanced Study Program, National Center for Atmospheric Research, Boulder, Colorado, USA

*5 Atmospheric Chemistry Division, National Center for Atmospheric Research, Boulder, Colorado,
USA*

*Corresponding author: m.t.lund@cicero.oslo.no

Abstract

We document the ability of the new generation Oslo chemistry-transport model, OsloCTM3, to accurately simulate present-day aerosol distributions. The model is then used with the new Community Emission Data System (CEDS) historical emission inventory to provide updated time series of anthropogenic aerosol concentrations and consequent direct radiative forcing (RFari) from 1750 to 2014.

Overall, the OsloCTM3 performs well compared with measurements of surface concentrations and remotely sensed aerosol optical depth. Concentrations are underestimated in Asia, but the higher emissions in CEDS than previous inventories result in improvements compared to observations. The treatment of black carbon (BC) scavenging in OsloCTM3 gives better agreement with observed vertical BC profiles relative to the predecessor OsloCTM2. However, Arctic wintertime BC concentrations remain underestimated, and a range of sensitivity tests indicate that better physical understanding of processes associated with atmospheric BC processing is required to simultaneously reproduce both the observed features. Uncertainties in model input data, resolution and scavenging affects the distribution of all aerosols species, especially at high latitudes and altitudes. However, we find no evidence of consistently better model performance across all observables and regions in the sensitivity tests than in the baseline configuration.

Using CEDS, we estimate a net RFari in 2014 relative to 1750 of -0.17 W m^{-2} , significantly weaker than the IPCC AR5 2011-1750 estimate. Differences are attributable to several factors, including stronger absorption by organic aerosol, updated parameterization of BC absorption, and reduced sulfate cooling. The trend towards a weaker RFari over recent years is more pronounced than in the IPCC AR5, illustrating the importance of capturing recent regional emission changes.

1 Introduction

Changes in anthropogenic emissions over the industrial period have significantly altered the abundance, composition and properties of atmospheric aerosols, causing a change in the radiative energy balance. The net energy balance change is determined by a complex interplay of different types of aerosols and their interactions with radiation and clouds, causing both positive (warming) and negative (cooling) radiative impacts. Global aerosols were estimated by the Intergovernmental Panel on Climate Change fifth assessment report (IPCC AR5) to have caused an effective radiative forcing (ERF) of -0.9 W m^{-2} over the industrial era from 1750 to 2011, but with considerable uncertainty (-1.9 to -0.1 W m^{-2}) [Boucher *et al.*, 2013]. This large uncertainty range arises from a number of factors, including uncertainties in emissions and the simulated spatiotemporal distribution of aerosols, their chemical composition and properties.

Historical emission estimates for anthropogenic aerosol and precursor compounds are key data needed for climate and atmospheric chemistry transport models in order to examine how these drivers have contributed to climate change. The Community Emissions Data System (CEDS) recently published a new time series of emissions from 1750 to 2014, which will be used in the upcoming CMIP6 [Hoesly *et al.*, 2018]. CEDS includes several improvements, including annual temporal resolution with seasonal cycles, consistent methodology between different species, and extending the time series to more recent years, compared to previous inventories and assessments [e.g., Lamarque *et al.*, 2010; Taylor *et al.*, 2012]. During the period from 2000 to 2014, global emissions of black carbon (BC) and organic carbon (OC) have increased, while nitrogen oxide (NO_x) emissions have been relatively constant after 2008, and sulfur dioxide (SO₂) emissions were back at 2000 levels in 2014, after a temporary increase [Hoesly *et al.*, 2018]. Furthermore, both CEDS and other recent emission inventories report considerably higher estimates of global BC and OC emissions in recent years than earlier inventories [Granier *et al.*, 2011; Klimont *et al.*, 2017; Lamarque *et al.*, 2010; Wang *et al.*, 2014]. The global trend in emissions is driven by a strong increase in emissions from Asia and Africa, and a decline in North America and Europe. Capturing such geographical differences is essential, as the distribution, lifetime and radiative forcing of aerosols depend on their location.

After emission or formation, particles undergo transport, mixing, chemical aging and removal by dry and wet deposition, resulting in a short atmospheric residence time, and a highly heterogeneous distribution in space and time. Consequently, accurate representation of observed aerosols remains challenging, and previous studies have shown that considerable diversity in the abundance and distribution of aerosols exist between global models. Bian *et al.* [2017] found that the atmospheric burden of nitrate aerosols differ by a factor of 13 between the models in AeroCom Phase III, caused by differences in both chemical and deposition processes. A smaller, but still considerable, model spread in the simulated burden of organic aerosols (OA) from 0.6-3.8 Tg was found by Tsigaridis *et al.* [2014]. It was also shown that OA concentrations on average were underestimated. There has been particular focus on BC aerosols over recent years. Multi-model studies have shown

variations in global BC burden and lifetime up to a factor of 4-5 [Lee *et al.*, 2013; Samset *et al.*, 2014]. Previous comparisons of modeled BC distributions with observations have also pointed to two distinct features common to many models: an overestimation of high altitude concentrations at low- to mid-latitudes and discrepancies in the magnitude and seasonal cycle of high-latitude surface concentrations (e.g., [Eckhardt *et al.*, 2015; Lee *et al.*, 2013; Samset *et al.*, 2014; Schwarz *et al.*, 2013]). As accurate representation of the observed aerosol distributions in global models is crucial for confidence in estimates of radiative forcing (RF), these issues emphasize the need for broad and up-to-date evaluation of model performance.

The diversity of simulated aerosol distributions, and discrepancies between models and measurements, stem from uncertainties in the model representation aerosol processing. Knowledge of the factors that control the atmospheric distributions is therefore needed to identify potential model improvements and need for further observational data, and to assess how remaining uncertainties affect the modeled aerosol abundances and, in turn, estimates of RF and climate impact. A number of recent studies have investigated the impact of changes in aging and scavenging processes on the BC distribution, focusing on aging and wet scavenging processes (e.g., [Bourgeois and Bey, 2011; Browse *et al.*, 2012; Fan *et al.*, 2012; Hodnebrog *et al.*, 2014; Kipling *et al.*, 2013; Lund *et al.*, 2017; Mahmood *et al.*, 2016]), resulting in notable improvements, at least for specific regions or observational data sets. However, with some notable exceptions [e.g., Kipling *et al.*, 2016], few studies have focused on impacts of scavenging and other processes on a broader set of aerosol species or the combined impact in terms of total aerosol optical depth (AOD).

Here we use the CEDS historical emission inventory as input to the chemistry-transport model OsloCTM3 to quantify the change in atmospheric concentrations over the period of 1750 to 2014. The OsloCTM3 is an update of the OsloCTM2, and includes several key changes compared to its predecessor. The significant existing model spread and sensitivity to process parameterizations underlines the need for careful and updated documentation of new model versions, and the increasing amount of available measurement data allows for improved evaluation. Before the model is used to quantify historical time series, we therefore evaluate the simulated present-day aerosol concentrations and optical depth against a range of observations. To get a first-order overview of how uncertainties in key processes and parameters affect the atmospheric abundance and distribution of aerosols in the OsloCTM3, we perform a range of sensitivity simulations. In addition to changes in the scavenging (solubility) assumptions, runs are performed with different emission inventories, horizontal resolution, and meteorological data. The impact on individual species and total AOD, as well as on the model performance compared with observations, is investigated. Finally, we present updated estimates of the historical evolution of radiative forcing due to aerosol-radiation interactions from pre-industrial to present, taking into account recent literature on aerosol optical properties. Section 2 describes the model and methods, while results are presented in Sect. 3 and discussed in Sect. 4. The conclusions are given in Sect. 5.

2 Methods

2.1 OsloCTM3

The OsloCTM3 is an offline global 3-dimensional chemistry-transport model driven by 3-hourly meteorological forecast data [Søvde *et al.*, 2012]. The OsloCTM3 has evolved from its predecessor OsloCTM2 and includes several updates to the convection, advection, photodissociation and scavenging schemes. Compared with OsloCTM2, the OsloCTM3 has a faster transport scheme, an improved wet scavenging scheme for large scale precipitation, updated photolysis rates and a new lightning parameterization. The main updates and subsequent effects on gas-phase chemistry were described in detail in Søvde *et al.* [2012]. Here we document the aerosols in OsloCTM3, including BC, primary and secondary organic aerosols (POA, SOA), sulfate, nitrate, dust and sea salt. The aerosol modules in OsloCTM3 are generally inherited and updated from OsloCTM2. The following paragraph briefly describes the parameterizations, including updates new to this work.

The carbonaceous aerosol module was first introduced by *Berntsen et al.* [2006] and has later been updated with snow deposition diagnostics [Skeie *et al.*, 2011]. The module is a bulk scheme, with aerosols characterized by total mass and aging represented by transfer from hydrophobic to hydrophilic mode at a constant rate. In the early model versions, this constant rate was given by a global exponential decay of 1.15 days. More recently, latitudinal and seasonal variation in transfer rates based on simulations with the microphysical aerosol parameterization M7 were included [Lund and Berntsen, 2012; Skeie *et al.*, 2011]. Previous to this study, additional M7 simulations have been performed to include a finer spatial and temporal resolution in these transfer rates. Specifically, the latitudinal transfer rates have been established based on experiments with 10 instead of four emission source regions and with monthly, not seasonal resolution. In OsloCTM3 the carbonaceous aerosols from fossil fuel and biofuel combustion are treated separately, allowing us to capture differences in optical properties in subsequent radiative transfer calculations (Sect. 2.4). In contrast to the OsloCTM2, OsloCTM3 treats POA instead of OC. If emissions are given as OC, a factor of 1.6 for anthropogenic emissions and 2.6 for biomass burning sources is used for the OC-to-POA conversion, following suggestions from observational studies [Aiken *et al.*, 2008; Turpin and Lim, 2001]. Upon emission, 20% of BC is assumed to be hydrophilic and 80% hydrophobic, while a 50/50 split is assumed for POA [Cooke *et al.*, 1999]. An additional update in this work is the inclusion of marine primary organic aerosols following the methodology by Gantt *et al.* [2015], where emissions are determined by production of sea spray aerosols and oceanic chlorophyll A. Monthly concentrations of chlorophyll A from the same year as the meteorological data is taken from the Moderate Resolution Imaging Spectroradiometer (MODIS; available from https://modis.gsfc.nasa.gov/data/dataproduct/chlor_a.php), while sea spray aerosols are simulated by the OsloCTM3 sea salt module. The climatological annual mean total emission

of marine POA is scaled to 6.3 Tg based on *Gantt et al.* [2015]. The scaling factor depends on the chosen sea salt production scheme (see below) and to some degree on the resolution; here we have used a factor of 0.5.

The formation, transport and deposition of SOA are parameterized as described by *Hoyle et al.* [2007]. A two product model (*Hoffmann et al.*, 1997) is used to represent the oxidation products of the precursor hydrocarbons and their aerosol forming properties. Precursor hydrocarbons which are oxidized to form condensable species include both biogenic species such as terpenes and isoprene, as well as species emitted predominantly by anthropogenic activities (toluene, m-xylene, methylbenzene and other aromatics). The gas/aerosol partitioning of semi-volatile inorganic aerosols is treated with a thermodynamic model [*Myhre et al.*, 2006]. The chemical equilibrium between inorganic species (ammonium, sodium, sulfate, nitrate and chlorine) is simulated with the Equilibrium Simplified Aerosol model (EQSAM) [*Metzger et al.*, 2002a; *Metzger et al.*, 2002b]. The aerosols are assumed to be metastable, internally mixed and obey thermodynamic gas/aerosol equilibrium. Nitrate and ammonium aerosols are represented by a fine mode, associated with sulfur, and a coarse mode associated with sea salt, and it is assumed that sulfate and sea salt do not interact through chemical equilibrium [*Myhre et al.*, 2006]. The sulfur cycle chemistry scheme and aqueous-phase oxidation is described by *Berglen et al.* [2004].

The sea salt module originally introduced by *Grini et al.* [2002] has been updated with a new production parameterization following recommendations by *Witek et al.* [2016]. Using satellite retrievals, *Witek et al.* (2016) evaluated different sea spray aerosol emission parametrizations and found the best agreement with the emission function from *Sofiev et al.* [2011] including the sea surface temperature adjustment from *Jaeglé et al.* [2011]. Compared to the previous scheme, the global production of sea salt is reduced, while there is an increase in the tropics. This will have an impact on the uptake of nitric acid in sea salt particles, consequently affecting NO_x, hydroxide (OH) and ozone levels. However, here we limit the scope to aerosols. The Dust Entrainment and Deposition (DEAD) model v1.3 [*Zender et al.*, 2003] was implemented into OsloCTM2 by *Grini et al.* [2005] and is also used in OsloCTM3. As a minor update, radiative flux calculations, required for determination of boundary layer properties in the dust mobilization parameterization [*Zender et al.*, 2003], now uses radiative surface properties and soil moisture from the meteorological fields.

Aerosol removal includes dry deposition and washout by convective and large-scale rain. Rainfall is calculated based on European Center for Medium-Range Weather Forecast (ECMWF) data for convective activity, cloud fraction and rain fall. The efficiency with which aerosols are scavenged by the precipitation in a grid box is determined by a fixed fraction representing the fraction of this box that is available for removal, while the rest is assumed to be hydrophobic. The parameterization distinguishes between large-scale precipitation in the ice and liquid phase, and the OsloCTM3 has a more complex cloud model than OsloCTM2 that accounts for overlapping clouds and rain based on *Neu and Prather* [2012]. When rain containing species falls into a grid box with drier air it will experience reversible evaporation. Ice scavenging, on the other hand, can

be either reversible or irreversible. For further details about large-scale removal we refer the reader to *Neu and Prather* [2012]. Convective scavenging is based on the Tiedtke mass flux scheme (Tiedtke 1989) and is unchanged from the OsloCTM2. The solubility of aerosols is given by constant fractions, given for each species and type of precipitation (i.e., large-scale rain, large-scale ice, and convective) (Table 2). Dry deposition rates are unchanged from OsloCTM2, but the OsloCTM3 includes a more detailed land use dataset (18 land surface categories at $1^\circ \times 1^\circ$ horizontal resolution compared to 5 categories at T42 resolution), which affects the weighting of deposition rates for different vegetation categories. Re-suspension of dry deposited aerosols is not treated.

2.2 Emissions

The baseline and historical simulations use the CEDS anthropogenic [*Hoesly et al.*, 2018; *Smith et al.*, 2015] and biomass burning (BB4CMIP) [*van Marle et al.*, 2017] emissions. The CEDS inventory provide monthly gridded emissions of climate-relevant greenhouse gases, aerosols and precursor species from 1750 to 2014 using a consistent methodology over time. Anthropogenic CEDS emissions are comparable to, but generally higher than, other existing inventories [*Hoesly et al.*, 2018]. Biogenic emissions are from the inventory developed with the Model of Emissions of Gases and Aerosols from Nature under the Monitoring Atmospheric Composition and Climate project (MEGAN-MACC) [*Sindelarova et al.*, 2014] and are held constant at the year 2010 level. Here we use the CEDS version released in 2016 (hereafter CEDSv16). In May 2017, after completion of our historical simulations, an updated version of the CEDS emission inventory was released after users reported year-to-year inconsistencies in the country/sector level gridded data. The emission totals were not affected, but there were occasional shifts in the distribution within countries (<http://www.globalchange.umd.edu/ceds/ceds-cmip6-data/>). The potential implications for our simulations are discussed below.

Two other emission inventories are also used. The ECLIPSEv5 emission dataset was created with the Greenhouse Gas - Air Pollution Interactions and Synergies (GAINS) model [*Amann et al.*, 2011] and provides emissions in 5 year intervals from 1990 to 2015, as well as projections to 2050 [*Klimont et al.*, 2017]. The 1990-2015 emission series was recently used to simulate changes in aerosols and ozone and their RF [*Myhre et al.*, 2017]. Here we only use emissions for 2010 in the sensitivity simulation.

The Representative Concentration Pathways (RCPs) [*van Vuuren et al.*, 2011] were developed as a basis for near- and long-term climate modeling and were used in CMIP5 and Atmospheric Chemistry and Climate Model Intercomparison Project (ACCMIP) experiments. While the four RCPs span a large range in year 2100 RF, emissions of most species have not diverged significantly in 2010 and we select the RCP4.5 for use here [*Thomson et al.*, 2011]. Table S1 summarized total global emissions of BC, OC, NO_x and SO₂ in 2010 in each of the three scenarios.

In the simulations with the ECLIPSEv5 and RCP4.5 inventories, biomass burning emissions are from the Global Fire Emission Database Version 4 (GFED4) [*Randerson et al.*, 2017]. The

BB4CMIP emissions are constructed with GFED4 1997-2015 emissions as a basis [van Marle *et al.*, 2017] and emissions in 2010 are similar in both datasets. Hence, any difference between the sensitivity simulations stems from differences in the anthropogenic inventory.

2.3 Simulations

Time slice simulations with CEDSv16 emissions for 1750, 1850 and from 1900 to 2014 are performed (every ten years from 1900-1980, thereafter every five years), one year with six months spin-up. The model is run with fixed year 2010 meteorological data and a horizontal resolution of 2.25x2.25 degrees (denoted 2x2), with 60 vertical layers. While Søvde *et al.* [2012] used meteorological data from the ECMWF IFS model cycle 36r1, we apply here meteorology from the ECMWF OpenIFS cycle 38r1 (<https://software.ecmwf.int/wiki/display/OIFS/>).

Additional model runs are performed to investigate the importance of differences in key processes for the aerosol distributions and model performance (Table 1). In addition to the CEDSv16 emissions, the model is run with ECLIPSEv5 and RCP4.5 emission inventories for anthropogenic emissions and GFEDv4 biomass burning emissions. Additionally, we perform simulations with 1.125x1.125 degrees (denoted 1x1) horizontal resolution. To investigate the importance of meteorology, the simulation with CEDSv16 emissions is repeated with meteorological data for year 2000 instead of 2010. Year 2000 is selected due to its opposite El Niño–Southern Oscillation (ENSO) index compared to 2010. Finally, three model runs are performed with increased and decreased aerosol removal by large-scale ice clouds and decreased aerosol scavenging by liquid (large-scale and convective) precipitation. To modify the scavenging, we tune the fixed fractions that control aerosol removal efficiency in the model (see Sect. 2.1). Table 2 summarizes fractions used in the baseline configuration and the three sensitivity tests. A decrease and increase in efficiency of 0.2 is adopted for scavenging of all aerosols by liquid clouds (except hydrophobic BC and POA) and ice clouds, respectively. Note that there is no test with increased removal by liquid clouds, as, with the exception of hydrophobic BC, POA and SOA, 100% efficiency is already assumed. For ice clouds we also reduce the efficiency to a fraction of 0.1, or 0.001 if the value is 0.1 in the baseline configuration. We note that these changes do not represent realistic uncertainty ranges based on experimental or observational evidence, as there are limited constraints in the literature, but are chosen to explore the impact of a spread in the efficiency with which aerosols act as ice and cloud condensation nuclei.

2.4 Radiative transfer

We calculate the instantaneous top-of-the atmosphere radiative forcing of anthropogenic aerosols due to aerosol-radiation interactions (RFari) [Myhre *et al.*, 2013b]). The radiative transfer

calculations are performed offline with a multi-stream model using the discrete ordinate method [Stamnes *et al.*, 1988]. The model includes gas absorption, Rayleigh scattering, absorption and scattering by aerosols, and scattering by clouds. The RFari of individual aerosols is obtained by separate simulations, where the concentration of the respective species is set to the pre-industrial level. The aerosol optical properties have been updated from earlier calculations using this radiative transfer model [Myhre *et al.*, 2007; Myhre *et al.*, 2009], in particular those associated with aerosol absorption. The Bond and Bergstrom [2006] recommendation of a mass absorption coefficient (MAC) for BC of around $7.5 \text{ m}^2 \text{ g}^{-1}$ for freshly emitted BC and an enhancement factor of 1.5 for aged BC was used previously. In the present analysis, we apply a parametrization of MAC from observations over Europe by Zanatta *et al.* [2016], where MAC depends on the ratio of non-BC to BC abundance. The mean MAC of BC from these observations around $10 \text{ m}^2 \text{ g}^{-1}$ at 630 nm [Zanatta *et al.*, 2016]. The measurements in Zanatta *et al.* [2016] represent continental European levels. For very low concentrations of BC, the formula given in Zanatta *et al.* [2016] provides very high MAC values. We have therefore set a minimum level of BC of $1.0\text{e-}10 \text{ g m}^{-3}$ for using this parameterization, and for lower concentrations we use Bond and Bergstrom [2006]. In addition, we have set a maximum value of MAC of $15 \text{ m}^2 \text{ g}^{-1}$ (637 nm) to avoid unrealistic high values of MAC compared to observed values. Organic matter has a large variation in the degree of absorption [e.g., Kirchstetter *et al.*, 2004; Xie *et al.*, 2017], from almost no absorption to a strong absorption in the ultraviolet region. Here, we have implemented absorbing organic matter according to refractive indices from Kirchstetter *et al.* [2004]. The degree of absorption varies by source and region and is at present inadequate quantified: Here we assume 1/3 of the biofuel organic matter and 1/2 of the SOA from anthropogenic volatile organic carbon (VOC) precursors. The remaining fractions of biofuel, fossil fuel and marine POA and SOA (anthropogenic and all natural VOCs) are assumed to be purely scattering organic matter. As these fractions are not sufficiently constrained by observational data and associated with significant uncertainty, we also perform calculations with no absorption by organic matter for comparison.

2.5 Observations

A range of observational datasets are used to evaluate the model performance in the baseline simulation. Note that we use the term “black carbon” in a qualitative manner throughout the manuscript to refer to light-absorbing carbonaceous aerosols. However, when comparing with measurements, we use either elemental carbon (EC) or refractive BC (rBC), depending on whether the data is derived from methods specific to the carbon content of carbonaceous aerosols or incandescence methods, in line with recommendations from Petzold *et al.* [2013].

Measured surface concentrations of EC, OC, sulfate and nitrate are obtained from various networks. For the US, measurements from IMPROVE (Interagency Monitoring of Protected Visual Environments) and CASTNET (Clean Air Status and Trends Network) are used. For Europe, data from EMEP (European Monitoring and Evaluation Programme) [Tørseth *et al.*, 2012] and

ACTRIS (Aerosols, Clouds and Trace gases Research InfraStructure) [Cavalli *et al.*, 2016; Putaud *et al.*, 2010] is used. EMEP and ACTRIS sites are all regional background sites, representative for a larger area. To broaden the geographical coverage we also compare the model output against additional observations from the CMA Atmospheric Watch Network (CAWNET) in China [Zhang *et al.*, 2012] and those reported in the literature from India (see Kumar *et al.* [2015] for more details). CASTNET, IMPROVE, EMEP and ACTRIS data is from year 2010, while CAWNET observations were sampled in 2006-2007 and the observational data base from India compiled by Kumar *et al.* [2015] cover a range of years. IMPROVE provides mass of aerosols using filter analysis of measurements of particulate matter with diameter of less than 2.5 micrometers (PM_{2.5}), while CASTNET uses an open-face filter pack system with no size restriction to measure concentrations of atmospheric sulfur and nitrogen species [Lavery *et al.*, 2009]. Mass of individual species from the CAWNET network is obtained from aerosol chemical composition analysis performed on PM₁₀ samples [Zhang *et al.*, 2012]. EMEP and ACTRIS measurements of EC and OC are in the PM_{2.5} range, whereas nitrate and sulfate measurements are filter-based with no size cutoff limit. Data resulting from EMEP and ACTRIS are archived in the EBAS data base (<http://ebas.nilu.no>) at NILU - Norwegian Institute for Air Research, and are openly available (see also Data availability).

Modeled AOD is evaluated against the Aerosol Robotics Network (AERONET). AERONET is a global network of stations measuring radiance at a range of wavelengths with ground-based sun-photometers, from which aerosol column burden and optical properties can be retrieved [Dubovik and King, 2000; Holben *et al.*, 1998]. The comparison with AERONET data was done using the validation tools available from the AeroCom data base hosted by Met Norway (<http://aerocom.met.no/data.html>). We also compare against AOD retrievals from MODIS-Aqua and Terra (level 3 atmosphere products, AOD550 combined dark target and deep blue, product version 6) [MOD08, 2018] and the Multi-angle Imaging SpectroRadiometer (MISR) (level 2 aerosol product, product version 4) [MISR, 2018].

Figure S1 depicts the locations of all the stations. For comparison with surface concentrations and AERONET AOD, the model data is linearly interpolated to the location of each station using annual mean, monthly mean (concentrations) or 3-hourly output (AOD), depending on the resolution of the observations. In the case of AERONET, high mountain stations (here defined as having an elevation higher than 1000 meter above sea level) are excluded following Kinne *et al.* [2013]. For comparison with observed OC surface concentrations, modeled OA is converted to OC using factor of 1.6 for POA and 1.8 for SOA. Unless measurements are restricted to the PM_{2.5} size range, the comparison includes both fine and coarse mode modeled nitrate (Sect. 2.1). Several statistical metrics are used to assess the model skill, including correlation coefficient (R), root mean square error (RMSE), variance and normalized mean bias (NMB).

The modeled vertical distribution of BC is compared with aircraft measurements of refractory BC (rBC) from the HIAPER Pole-to-Pole Observations (HIPPO) campaign [Wofsy *et al.*, 2011].

Vertical profiles of BC from OsloCTM2 have been evaluated in several previous studies (e.g., *Samset et al.* [2014]) and a more thorough comparison of OsloCTM3 results against a broader set of campaigns is provided by *Lund et al.* [2018]. In the present analysis we focus on data from the third phase (HIPPO3) flights, the only phase that was conducted in 2010, i.e., the same year as our sensitivity simulations. Model data is extracted along the flight track using an online flight simulator. The data is separated into five latitude regions and vertical profiles constructed by averaging observations and model output in 13 altitude bins.

3 Results

We first document the aerosol distributions simulated in the baseline model configuration, focusing on the anthropogenic contribution, and compare with observations, multi-model studies and results from the sensitivity tests. With the present-day model performance evaluated, we then present the updated historical development of RFari of anthropogenic aerosols.

3.1 Evaluation of present-day aerosol distributions

The global mean aerosol burdens and atmospheric residence times (ratio of burden to total wet plus dry deposition) in the baseline simulation are summarized in Table 3 (top row), with spatial distribution shown in Fig. S2. Compared to results from the AeroCom III experiment, the OsloCTM3 sulfate burden of 5.4 mg m^{-2} estimated here is about 50% higher than the multi-model mean of 3.5 mg m^{-2} and 35% higher than OsloCTM2 [*Bian et al.*, 2017]. While the total SO_2 emission is only 5% higher in the present study than in the OsloCTM2 AeroCom III simulation, the atmospheric residence time of sulfate is 50% longer, suggesting that the burden difference is mainly attributable to changes in the parameterization of dry and large-scale wet deposition in OsloCTM3 (Sect. 2.1). The nitrate burden is nearly a factor three higher than both the AeroCom multi-model mean and OsloCTM2 burden, and higher than all nine models contributing in AeroCom III [*Bian et al.*, 2017]. This is mainly due to a higher burden of coarse mode nitrate aerosols, associated with less efficient scavenging of sea salt in OsloCTM3 than OsloCTM2. The global budgets of OA simulated by the AeroCom II models was analyzed by *Tsigaridis et al.* [2014]. The burden of OA in the OsloCTM3 of 3.4 mg m^{-2} is close to their multi-model mean of 3.1 mg m^{-2} and 25% higher than the OsloCTM2. The OsloCTM3 estimate includes the contribution from marine OA emissions (Sect. 2.1), which may explain part of the difference as marine OA was included in some of the AeroCom II models, but not OsloCTM2. However, the marine POA only contributes around 3% to the total OA. Additionally, the residence time of OA of 5.3 days is longer than in the OsloCTM2 AeroCom II experiment. The global BC burden of 0.23 mg m^{-2} is also close to the mean of the AeroCom II models of 0.25 mg m^{-2} [*Samset et al.*, 2014]. We note that different emission inventories were used in the AeroCom experiments and the present analysis, however,

the comparison shows that the aerosol burdens simulated by OsloCTM3 fall within the range of existing estimates from global models.

Figure 1 shows results from the baseline OsloCTM3 simulation against annual mean measured surface concentrations of EC, OC, sulfate and nitrate in Europe, North America and Asia. Overall, the OsloCTM3 shows a high correlation of 0.8-0.9 with measured surface concentrations. There is a general tendency of underestimation by the model, with the lowest NMB and RMSE for BC and nitrate (-23%) and the highest for sulfate (-52%). There are, however, notable differences in model performance between data sets in different regions, as seen from Table S2. For all species, the NMB and RMSE are highest for measurements in China. For instance, excluding the CAWNET measurements, reduces the NMB for sulfate in Fig. 1 from -52% to -31% (not shown). In contrast, the correlation with CAWNET observations is generally similar to, or higher than, other regions/networks. In the case of BC and nitrate, the model slightly overestimates concentrations in Europe and North America, but underestimates Asian measurements. The best overall agreement is generally with IMPROVE observations in North America. Differences in instrumentation between different networks can affect the evaluation. *Lavery et al.* [2009] found that measurements from CASTNET typically gave higher nitrate surface concentrations than values obtained from co-located IMPROVE stations, which could partly explain the NMB of opposite sign in these two networks in Table S2. For BC, we also include measurements from across India compiled by *Kumar et al.* [2015]. This is a region where emissions have increased strongly, but where evaluation of the model performance so far has been limited due to availability of observations. The model underestimates concentrations with a NMB of -43%, however, the correlation of 0.60 is similar to the comparison with data from China and higher than the other regions. An examination of the monthly concentrations (Fig. S3) shows that the largest discrepancies occur during winter, with the largest bias found for measurements in North East India. One possible reason could be missing or underestimated emission sources. This finding is similar to the comparison of measurements against WRF-chem by *Kumar et al.* [2015]. The seasonality of BC concentrations has also been an issue at high northern latitudes, where earlier versions of the OsloCTM strongly underestimated winter and springtime surface concentrations at Arctic stations [*Lund et al.*, 2017; *Skeie et al.*, 2011], similar to many other models [*Eckhardt et al.*, 2015]. This Arctic underestimation persists in the current version of the model. Seasonal differences exist also in other regions, but not consistently across measurement networks. Compared with EC measurements from EMEP/ACTRIS the correlation is poorer during winter and spring, and the model underestimate concentrations in contrast to a positive NMB in summer and fall. However, due to the relatively low number of stations, these values are sensitive to a few stations with larger measurement-model discrepancies. For both IMPROVE and EMEP/ACTRIS, the model underestimation of sulfate is larger during summer and fall, but with opposite seasonal differences in correlation. In general, the number of stations and evaluation of data from only one year limits the analysis of seasonal variations.

We do not evaluate ammonium concentrations in the present analysis, as that requires a detailed discussion of the nitrate and sulfate budgets, which has been covered by the recent multi-model evaluation by *Bian et al.* [2017] based on an AeroCom Phase III experiment, in which the OsloCTM3 participated. Results showed that most models tend to underestimate ammonium concentrations compared to observations in North America, Europe and East Asia, with a multi-model mean bias and correlation of 0.886 and 0.47, respectively. The OsloCTM3 shows good agreement with ammonium measurements in North America, but has a bias and correlation close to the model average in the other two regions.

In May 2017, after completion of our historical simulations, an updated version of the CEDS emission inventory was released after an error in the code was reported (see Sect. 2.2). This resulted in occasional shifts in the spatial distribution of emissions within countries with large spatial extent (e.g., USA and China). Since the emission totals were not affected, the impact on our RFari estimates is likely to be small, but shifts in the emission distribution could influence the model evaluation, in particular for surface concentrations. While repeating all simulations would require more resources, we have repeated the year 2010 and 1750 runs. Figure S4 shows the comparison of modeled concentrations against IMPROVE measurements with the two emission inventory versions, CEDSv16 and CEDSv17. In the case of BC, the comparison shows a 5% higher correlation and 15% lower RMSE with the CEDSv17 than CEDSv16. A similar improvement is found for nitrate, with 26% higher correlation and 12% lower RMSE, while in the case of OC and sulfate, the difference is small (< 5%). Smaller differences of between 2-10% are also found in the comparison against measurements in Europe and Asia (not shown). Hence, using the updated version of the emission inventory has an effect on the model performance in terms of surface concentrations, but without changing the overall features or conclusions. The net RFari in 2010 relative to 1750 is 2% stronger with the CEDSv17 inventory, a combined effect of slightly higher global BC burden and lower burdens of sulfate and OA.

As shown in Table S2, the model overestimate surface concentrations in some regions and underestimate them in others. Compensating biases can influence the evaluation of total AOD. Moreover, the biases differ in magnitude between different species. Moving one step further, we therefore examine the average aerosol composition in the three regions where this is possible with our available measurements. Figure 2 shows the relative contribution from different aerosols species to the total mass in the IMPROVE, EMEP, ACTRIS and CAWNET measurements and the corresponding model results. The number of available aerosol species varies between the measurement networks and we include sea salt from IMPROVE and ammonium from CAWNET. Additionally, the number of stations where simultaneous measurements of all species were available also differ substantially, with 16 for CAWNET, 5 for EMEP/ACTRIS and 172 for IMPROVE. Overall, the relative composition is well represented by the model. The agreement is particularly good for the IMPROVE network. Compared to measurements from CAWNET, the model has a lower relative contribution from OC and more sulfate. In the case of Europe, nitrate aerosols also constitute a significantly larger fraction in the model than in the observations. The

evaluation of nitrate is complicated by possible differences in the detection range of instrumentation compared to the size of the two nitrate modes in the model (Sect. 2.1). The comparison against EMEP nitrate data includes both coarse and fine mode modeled nitrate. Excluding the coarse mode, the fraction of total mass attributable to nitrate decreases from 43% to 28%, which is much closer to the observed 30% contribution. However, this affects the comparison in Figure 1, resulting in a negative NMB of -34%, compared to -23% when including both coarse and fine mode. This suggests that part, but not all, of the nitrate represented as a coarse mode in the model is measured by the instrument, pointing to a need for a more sophisticated size distribution in the model to make better use of available observations. The low number of available stations from EMEP/ACTRIS could also be an important factor.

Next, we examine total AOD. Figure 3 shows modeled AOD and aerosol absorption optical depth (AAOD), AOD retrieved from MODIS-Aqua and comparison of modeled AOD with AERONET observations. Modeled global, annual mean AOD and AAOD is 0.13 (Fig. 3a) and 0.0051 (Fig. 3b), respectively. The overall spatial pattern of modeled AOD agrees well with MODIS (Fig. 3c), however, the latter gives a higher global mean of 0.16 and clearly higher values in North India and parts of China, as well as Central Africa. These peak values are similar to MODIS-Terra, but less pronounced in the AOD retrieved from MISR (Fig. S5), illustrating important differences between different remote sensing products. Nevertheless, an underestimation of modeled AOD in Asia is consistent with results from the evaluation of surface concentrations and can also be seen in the comparison against AERONET, as discussed below. The OsloCTM3 shows a good agreement with measured AOD from the AERONET network, with an overall correlation of 0.82 and RMSE of 0.11, when using monthly mean data from 266 stations (Fig. 3d). Note that the modeled global mean AOD is 0.13, but the model mean at the AERONET stations is 0.175 (Fig. 3d) and has only a NMB of -11.8%. Many of the AERONET stations tend not to be regional background sites, but can be influenced by local pollution (e.g., Wang *et al.* [2018]).

However, there are notable regional differences in model performance. Fig. S6 compares modeled AOD against AERONET stations in Europe, North America, India and China separately. The best agreement is found for Europe and North America, with NMB of -0.4% and -13%, respectively, and RMSE of approx. 0.05. The correlation is higher for North America (0.71) than Europe (0.63). A relatively high correlation of 0.71 is also found for stations in China. However, the NMB and RMSE is higher (-34.5% and 0.25). There are significantly fewer observations for comparison with modeled AOD over India, but the ones available give NMB and RMSE on the same order of magnitude as for China, but a lower correlation (0.45).

Ground-based measurements can also provide information about column absorption aerosol optical depth (AAOD). Such information has been used to constrain the absorption of BC and provide top-down estimate of the direct BC RF (e.g., [Bond *et al.*, 2013]). However, retrieval and application of AERONET AAOD is associated with a number of challenges and uncertainties (e.g., [Samset *et al.*, 2018]), hence such an evaluation is not performed here.

Recent literature has pointed to important representativeness errors arising when constraining models using observations due to the coarse spatial and temporal scales of global models compared with the heterogeneity of observations. *Schutgens et al.* [2016a] found differences in RMSE of up to 100% for aerosol optical thickness when aggregating high resolution model output over grid boxes representative of the resolution of current global models compared to small areas corresponding to satellite pixels. Smaller, but notable, differences of up to 20% were found when monthly mean model data was used, as in the present analysis. However, that did not account for issues related to temporal collocation, which can also introduce considerable errors [*Schutgens et al.*, 2016b]. In a recent study, *Wang et al.* [2018] found a spatial representativeness error of 30% when constraining AAOD modeled at a 2°x2° horizontal resolution against AERONET retrievals. However, further work is needed to investigate whether similar biases exist for AOD.

3.2 Sensitivity of aerosols distributions to model input and process parameterization

As shown in the section above, the OsloCTM3 performs well compared against observed AOD. Still, a number of factors influence the simulated distributions of individual aerosol species. To assess the importance of key uncertainties for modeled distributions and model performance, we perform a range of sensitivity simulations (Table 1) to examine the importance of emission inventory, scavenging assumptions (Table 2), meteorological data and resolution for the modeled aerosol distributions and model performance.

Global aerosol burdens and AOD in each sensitivity run are summarized in Table 3 (corresponding atmospheric residence times are given in Table S3). The BC burden is particularly sensitive to reduced scavenging by large-scale ice clouds (LSIDEC), resulting in a 40% higher burden compared to the baseline. In contrast, an equal increase in the scavenging efficiency (LSIINC) result in a decrease in burden of only 9%, while decreased scavenging by liquid precipitation (SOLDEC) gives a 13% higher burden. The lower BC emissions in the ECLv5 and CMIP5 inventories give a global BC burden that is 9 and 22% lower, respectively. For sulfate, ammonium and OA, we also find the largest burden changes in the LSIDEC case, followed by SOLDEC. The change in the LSIDEC is particularly large for OA and is driven by changes in SOA. For SOA, the changes are determined not only by modifying the scavenging, but also by changes in POA concentrations, which gas-phase secondary organics can partition onto. Increasing the horizontal resolution results in a slightly higher burden for all species, except sea salt.

While sensitivity tests may give similar changes in the total global burdens, the spatial distribution of changes can differ substantially. Figure 4 shows the ratio of AOD and total burden by species and altitude in each sensitivity simulation to the baseline. As expected, varying the emission inventories results in changes that are largely confined to the main source regions (Figs.4a,b). Using the CMIP5 inventory results in considerably lower concentrations over Asia, the Middle East and North Africa, reflecting the higher emissions in the more recent inventory. Over central

North America the AOD is higher, mainly due to more ammonium nitrate, whereas the higher AOD over Eastern Europe and part of Russia is a result of higher sulfate concentrations. Similar characteristics are found when using ECLv5, but the relative differences are smaller. Reducing or increasing the large-scale ice cloud scavenging gives the largest relative changes in AOD at high latitudes, while changes in the solubility assumption for liquid precipitation affects AOD most over Asia, where aerosol burdens are high, and around the equator where convective activity is strong. In general, the burden of BC, OA and dust is significantly affected by changes in the scavenging assumptions, while nitrate responds more strongly to different emission inventories, likely due to the complicated dependence on emissions of several precursors and competition with ammonium-sulfate. We also note that at higher altitudes the absolute differences in the burden of nitrate are small. Changes in AOD resulting from using different meteorological input data are more heterogeneous and are most notable in regions where effects of choosing data from years with opposite ENSO phase are expected, e.g., west coast of South America and South East Asia. There is also a notable change in the Atlantic Ocean, where mineral dust is a dominating species. The meteorological data can affect production, deposition and transport of dust directly, as well as indirectly through ENSO-induced teleconnections as suggested by e.g., *Parhi et al.* [2016].

For BC, OA and dust, the largest impact relative to the baseline are seen above 600 hPa in the LSIDE case. Change in LSIDE are also important in the case of sulfate and sea salt, but occur at lower altitudes. In contrast to the other aerosol species, differences in emission inventories are most important for nitrate. In a recent study, *Kipling et al.* [2016] investigated factors controlling the vertical distribution of aerosols in the HadGEM3-UKCA. It was found that in-cloud scavenging was very important in controlling the vertical mass concentration of all species, except dust. For dust, it was also found that dry deposition and sub-cloud processes played key roles, processes not examined in the present analysis. Moreover, *Kipling et al.* [2016] performed sensitivity simulations by switching transport and scavenging on and off to get the full effect of a given process, while we perform smaller perturbations to investigate uncertainties. Here we find significant impacts of changes in ice-cloud removal efficiency (Table 2) on the vertical distribution of BC, OA and dust, while large-scale liquid and convective precipitation is more important for sea salt and nitrate

Our sensitivity tests show that changes in input data, resolution or scavenging can lead to notable changes in the aerosol distributions. The next question is then how these changes affect model performance compared to observations. Figure 5a compares modeled and measured surface concentrations of BC, OC, sulfate and nitrate in each simulation using all observations in Fig. 1. For BC, the sensitivity tests have little or no impact on correlation, but there is a markedly better agreement in terms of standard deviation (i.e., model becomes closer to observations) for CEDSv16/CMIP6 compared to RCP/CMIP5, reflecting the higher emissions in the former. Similar, but smaller, effects are also found for the other species. The improvement from RCP/CMIP5 to CEDSv16/CMIP6 is especially seen for measurements in Asia. A higher resolution is also found to reduce the bias, in particular for BC. Figure 5b shows the comparison against AERONET AOD

in each sensitivity simulation. Again, there is a higher correlation and lower bias in the 1x1RES run than in the baseline, while the opposite is found in the RCP/CMIP5 and ECLv5 cases. For both observables, the improvement in the 1x1RES simulation may result from a better sampling at a finer resolution, improved spatial distribution or a combination. The most pronounced changes results from using meteorological data from year 2000, in which case the correlation is reduced from around 0.8 to 0.7.

For both observables, the difference in model performance between the baseline and scavenging sensitivity tests is small. This may partly be an effect of the geographical coverage of stations; the majority of measurements are from stations in more urban regions, whereas simulated burden changes occur in remote regions, particularly at high latitudes and altitudes (Fig. 4). We therefore also perform evaluations against AOD from regional sub-sets of AERONET stations. Ten of the AERONET stations used in the present analysis are located north of 65°N (Fig. S1). A comparison of monthly mean simulated AOD in each of the sensitivity runs against observations in this region shows the best agreement with the baseline simulation and with the ECLv5 emission inventory, with a considerably higher bias when scavenging parameters are modified (Fig. S7a). This is particularly the case in the LSIDE run, where concentrations of all species increase at high latitudes compared to the baseline (Fig. 4). In contrast, the reduced concentrations in LSIINC, results in a negative bias. We note that most of these stations have missing values in the winter months, which is when the model underestimate BC concentrations in the Arctic, hence limiting the evaluation. Decreased scavenging efficiency also leads to a higher bias than in the baseline for observations in Europe and North America (not shown). In Asia, where the model already underestimates aerosols in the baseline configuration, the bias is reduced since concentrations increase. However, differences are smaller than north of 65°N. Moreover, given the notable exacerbation in model performance in other regions, it is likely that other sources of uncertainty (e.g., emissions) are more important for the model-measurement discrepancies in Asia. A similar comparison is performed for 15 AERONET stations located in North Africa and the Middle East (Fig. S7b), where the dust influence is strong. Changing the meteorological year and reducing scavenging results in higher dust burdens (Table 3). Again, the agreement is better in the baseline run than in these sensitivity runs. In particular, the METDATA run result in a higher bias and a lower correlation, which is not surprising as dust production depends also on meteorological conditions. The changes compared to the baseline CEDSv16/CMIP6 simulation cannot be entirely attributed to differences in dust concentrations, as seen from the RCP/CMIP5 and ECLv5 simulations where the dust production is equal to the baseline. Several studies have pointed to the importance of spatial resolution for improved model performance compared to observations (e.g., [Sato *et al.*, 2016; Schutgens *et al.*, 2017; Schutgens *et al.*, 2016a; Wang *et al.*, 2016]). Wang *et al.* [2016] found significant reductions in NMB of BC AAOD relative to AERONET when using a high resolution (10 km) emission data and model output. In our analysis, moving from 2°x2° to 1°x1° horizontal resolution also results in a slightly higher correlation and reduced bias and errors when compared to all AERONET stations (Fig. 5b). The impact is largest for AOD in China and India, the NMB is reduced (from -34% and -24% (Fig. S6) to -20% and -10%, respectively).

However, the opposite effect is found for AERONET stations in Europe and North America. Of course, the $1^\circ \times 1^\circ$ resolution is still very coarse compared to the grid sizes used in the abovementioned studies.

Changes away from near-source areas are also evaluated in terms of BC concentrations by a comparison with observed vertical distribution from the HIPPO3 campaign, where remote, marine air over the Pacific was sampled across all latitudes (Sect. 2.5). To limit the number of model runs, we focus on only one phase of the HIPPO campaign here, but a more comprehensive evaluation of OsloCTM3 vertical BC distribution against aircraft measurements was performed by *Lund et al.* [2018]. Figure 6 shows observed average vertical BC concentration profiles against model results from each sensitivity test. The OsloCTM3 reproduces the vertical distribution well in low and mid-latitudes over the Pacific in its baseline configuration, although near-surface concentrations in the tropics are underestimated. This is a significant improvement over the OsloCTM2, where high-altitude concentrations in these regions typically were overestimated. The baseline configuration of OsloCTM3 includes updates to the scavenging assumptions based on previous studies investigating reasons for the high-altitude discrepancies (e.g., [*Hodnebrog et al.*, 2014; *Lund et al.*, 2017]). At high northern and southern latitudes, the model underestimates the observed vertical profiles in the baseline. Increasing the model resolution does not have any notable impact on the vertical profiles. There is a notable increase in high-latitude concentrations when large-scale ice cloud scavenging is decreased. However, there is a simultaneous exacerbation of model performance in the other latitude bands, pointing to potential tradeoffs when tuning global parameters, as also illustrated by *Lund et al.* [2017]. Due to the significant altitude dependence of the radiative effect of BC (e.g., [*Samset et al.*, 2013]), high altitude overestimations will contribute to uncertainties in BC RFari. We also note that HIPPO3 was conducted in March/April: Comparison with aircraft measurements from other seasons show a smaller underestimation at high latitudes [*Lund et al.*, 2018].

3.3 Pre-industrial to present-day aerosols

With confidence in the model ability to reasonably represent current aerosol distributions established, we next present an updated historical evolution of anthropogenic aerosols from pre-industrial to present-day, and the consequent direct radiative effect (RFari) (Sect. 2.4). Figure 7 shows the net change in total aerosol load from 1750 to 2014. Full times series by species are given in Table S4. To keep in line with the terminology used in the IPCC AR5, we now separate out biomass burning BC and POA in a separate species “biomass”. We also note that only the fine mode fraction of nitrate contributes to the RFari and is included in Fig. 7. To illustrate the contributions from additional emissions during the past 14 years, we also include the 2000-1750 difference. The values from the present study are also compared with results from the AeroCom II models [*Myhre et al.*, 2013a], where emissions over the period 1850 to 2000 from *Lamarque et al.* [2010] were used.

The most notable difference compared to the AeroCom II results is seen for biomass aerosols. Biomass burning emissions have high interannual variability and this affects the analysis. While the 1750-2014 difference is 0.23 mg m^{-2} , taking the difference between year 1750 and 2000 (black asterisk) results in a net change of only 0.03 mg m^{-2} . There is also a much larger change in the burden of biomass aerosols in the AeroCom experiments, reflecting a more than 100% higher emissions in 2000 compared to 1850 *Lamarque et al.* [2010] inventory. However, biomass aerosols comprises both scattering OA and absorbing BC and, as seen below, these nearly cancel in terms of RFari. Changes in sulfate and OA from pre-industrial to 2000 are slightly higher in the present analysis than in AeroCom II, and the influence of additional emissions since 2000 is seen. The OsloCTM3 is well below the AeroCom multi-model mean for nitrate. The OsloCTM2 was found to be in the low range, but the multi-model was also influenced by some models giving high estimates [*Myhre et al.*, 2013a]

Using the CEDSv16 emissions, we estimate a net RFari from all anthropogenic aerosols in 2014 relative to 1750 of -0.17 W m^{-2} . The RFari from sulfate is -0.30 W m^{-2} , while the contributions from OA (combined fossil fuel plus biofuel POA and SOA), nitrate and biomass aerosols are smaller in magnitude of -0.09 , -0.02 and -0.0004 W m^{-2} , respectively. The RFari due to fossil fuel and biofuel BC over the period is 0.31 W m^{-2} .

Figure 8a shows the time series of RFari by component, as well as the net, in the present analysis (solid lines), and corresponding results reported in the IPCC AR5 (dashed lines). The net RFari over time is mainly determined by the relative importance of compensating BC and sulfate RFari. The most rapid increase in BC RFari is seen between 1950 and 1990, as emissions in Asia started to grow, outweighing reductions in North America and Europe [*Hoesly et al.*, 2018]. After a period of little change between 1990 and 2000, the rate of change increases again over the past two decades, following strong emission increases in Asia and South Africa. Similarly, cooling contribution from sulfate aerosols strengthened from around mid-century. However, in contrast to BC, the evolution is fairly flat after 1990. The last 20 years has seen a continuous reduction in sulfur dioxide (SO_2) emissions in Europe, from around 30 to 5 Tg yr^{-1} in CEDSv16, with a similar trend in North America. While emissions in China continue to increase well into the 2000s, a stabilization is seen after 2010, following introduction of stricter emission limits as part of a program to desulfurize power plants [*Klimont et al.*, 2013]. During the same period, emissions in India have risen. However, the net global SO_2 emission trend over the past few years is a slight decline [*Hoesly et al.*, 2018]. This development is reflected in the net RFari, which reaches its peak (i.e., strongest negative value) around 1990 and gradually becomes weaker thereafter. This trend is more pronounced in the present analysis than in the IPCC AR5 estimates, where the forcing due to sulfate is more flat in recent decades, suggesting that projected emission estimates underestimated recent decreases in SO_2 . The minimum net RFari value is also reached later in the latter. Moreover, a recent study suggests that current inventories underestimate the decline in Chinese SO_2 emissions and estimate a 75% reduction since 2007 [*Li et al.*, 2017]. In this case, the

weakening trend could be even stronger than estimated here. The insert in Fig. 8a focuses on recent estimates of total RFari over the period 1990-2015. Using the ECLv5 emission inventory, *Myhre et al.* [2017] found a global mean RFari due to changes in aerosol abundances over the period 1990-2015 of $0.05 (\pm 0.04) \text{ W m}^{-2}$. Our results using CEDSv16 emissions are in close agreement with these findings.

Over the past decades, there has been shift in emissions, from North America and Europe to South and East Asia. This is also reflected in the zonally averaged net RFari over time in Fig. 8b. RFari declined in magnitude north of 40°N after 1980, with particularly large year-to-year decreases between 1990 and 1995, and from 2005 to 2010, and strengthened in magnitude between 10° - 30°N . The RFari also strengthened in the Southern Hemisphere subtropical region, reflecting increasing emission in Africa and South America after 1970. However, the peak net RFari is considerably weaker in 2014 than the peak in 1980. This mainly is due to fact that simultaneously with the southwards shift, the sulfate burden has declined, while the BC burden has increased steadily at the same latitudes, resulting in a weaker net RF. The past decade, the net RFari has switched from negative to positive north of 70°N , due to a combination of stronger positive RF of BC and from biomass burning aerosols.

Table S5 shows changes in burden, AOD, AAOD, RFari, and normalized RF over the period 1750-2010 for individual aerosol components and the net RFari. Compared to earlier versions of OsloCTM [*Myhre et al.*, 2009; *Myhre et al.*, 2013a] the normalized RF with respect to AOD is lower because of short lifetime of BC resulting in smaller abundance of BC above clouds, whereas normalized RF with burden is comparable to earlier estimates because of higher MAC compensate for short lifetime of BC. Weaker normalized RF of OA (POA and SOA) than earlier OsloCTM versions is due to the inclusion of absorbing OA.

In the present study we have used an updated parameterization of BC absorption based on *Zanatta et al.* [2016] (Sect. 2.4), which takes into account the ratio of non-BC-to-BC material and results in a MAC of $12.5 \text{ m}^2 \text{ g}^{-1}$ at 550 nm. This is 26% higher than the $9.94 \text{ m}^2 \text{ g}^{-1}$ using the approach from *Bond and Bergstrom* [2006]. Using the latter, we estimate a BC RFari in 2014 relative to 1750 of 0.23 W m^{-2} , 25% lower than the 0.31 W m^{-2} calculated based on *Zanatta et al.* [2016]. These results emphasize the importance of assumptions and uncertainties related to the BC absorption.

The magnitude of RFari by scattering aerosols is sensitive to assumptions about absorption by organic aerosols, so-called brown carbon (BrC). Observational studies have provided evidence for the existence of such particles, and modeling studies suggest they could be responsible for a substantial fraction of total aerosol absorption, although the spread in estimates is wide (e.g., *Feng et al.* [2013] and reference therein). In the present study we assume a considerable fraction of absorption by OA (Sect. 2.4). Assuming purely scattering aerosols, the RFari from OA is -0.13 W m^{-2} ; accounting for BrC absorption this is weakened to -0.09 W m^{-2} . Splitting total OA RFari into

contributions from primary and secondary aerosols, we find that purely scattering POA gives a RFari of -0.07 W m^{-2} compared to -0.06 W m^{-2} with absorption. The corresponding numbers for SOA are -0.06 and -0.03 W m^{-2} . This indicates that in OsloCTM3, the absorbing properties of SOA are relatively more important than for POA. This is likely due to the generally higher altitude of SOA than POA (Fig. S8) in combination with the increasing radiative efficiency of absorbing aerosols with altitude [Samset *et al.*, 2013]. However, due to the weaker overall contributions from OA, our results indicate that differences in parameterization of BC absorption can be more important than uncertainties in absorption by BrC for the net RFari.

4 Discussion

Our estimate of total net RFari in 2014 relative to 1750 is weaker in magnitude than the best estimate for the 1750-2010 period reported by IPCC AR5. The difference is due to a combination of factors, including weaker contributions from both cooling aerosols and BC. Despite considerably higher BC emissions in the CEDSv16 inventory compared to older inventories, we calculate a weaker BC RFari than reported in AR5, hence going in the opposite direction of explaining the difference to IPCC AR5 total RFari. The IPCC AR5 best estimate for fossil fuel and biofuel BC of 0.4 (0.05 to 0.8) W m^{-2} [Boucher *et al.*, 2013] was based mainly on the two studies by Myhre *et al.* [2013a] and Bond *et al.* [2013], who derived estimates of BC RFari of 0.23 (0.06 to 0.48) W m^{-2} and 0.51 (0.06 to 0.91) W m^{-2} , respectively. The spread between the two is largely attributed to methodological differences: Bond *et al.* [2013] used an observationally weighted scaling of results to match those based on AERONET AAOD, which was not adopted by Myhre *et al.* [2013a]. Such ad-hoc adjustments typically result in higher estimates (Wang *et al.* [2018] and references therein). Moreover, a recent study by Wang *et al.* [2018] suggest that representativeness error arising when constraining coarse resolution models with AERONET AAOD could result in a 30% overestimation of BC RFari, which explains some of the differences between bottom-up and observationally constrained numbers. The BC RFari estimate from the present study is around 20% higher than the AeroCom multi-model mean from Myhre *et al.* [2013a] when calculated over the same period 1850-2000. This reflects the higher emissions in the CEDSv16 emission inventory than in Lamarque *et al.* [2010], as well as a higher MAC.

A significant range from -0.85 to $+0.15 \text{ W m}^{-2}$ surrounds the central RFari estimate of -0.35 W m^{-2} from IPCC AR5 [Boucher *et al.*, 2013], caused by the large spread in underlying simulated aerosol distributions. Deficiencies in the ability of global models to reproduce atmospheric aerosol concentrations can propagate to uncertainties in RF estimates. As shown in Sect. 3, the OsloCTM3 generally lies close to or above the multi-model mean of anthropogenic aerosol burdens from recent studies and is found to perform reasonably well compared with observations and other global models, with improvements over the predecessor OsloCTM2. In particular, recent progress towards constraining the vertical distribution of BC concentrations has resulted in improved agreement between modeled and observed vertical BC profiles over the Pacific Ocean with less of

the high-altitude overestimation seen in earlier studies. However, as shown by *Lund et al.* [2018], there are discrepancies compared to recent aircraft measurements over the Atlantic Ocean. A remaining challenge is the model underestimation of Arctic BC concentrations. However, this is seen mainly during winter and early spring, when the direct aerosol effect is small due to lack of sunlight. In contrast, the higher emissions in the CEDSv16 inventory also results in an improved agreement with BC surface concentrations over Asia.

In general, we find lower surface sulfate concentrations in the model compared with measurements. This could contribute to an underestimation of the sulfate RFari, which is weaker in the present study than in IPCC AR5. An underestimation of observed AOD in Asia is also found, however, the implication of this bias on RF is not straightforward to assess, as it is complicated by the mix of absorbing and scattering aerosols. We note that the global mean sulfate burden is higher in the OsloCTM3 than in most of the global models participating in the AeroCom III experiment (Sect. 3.1, *Bian et al.* [2017]), and that the OsloCTM3 performs similarly to or better than other AeroCom Phase III models in terms of nitrate and sulfate surface concentrations, at least for measurements from CASTNET [*Bian et al.*, 2017]. Nevertheless, the model diversity in simulated nitrate and sulfate remains large and, although all models capture the main observed features in concentrations, further work is needed to resolve the differences and improve model performance for these species.

While a comprehensive quantitative uncertainty analysis of the updated RFari estimate is not possible within the scope of this study, we explore the order of magnitude uncertainties due to “internal” factors such as scavenging parameterizations and model resolution by performing sensitivity tests. Changes in global burden on the order of 10-20%, and up to 65%, were found (Sect. 3.2). However, compared to observations of surface concentrations in near-source regions, total AOD and vertical distribution of BC concentrations, we saw that the model generally performed the best in its baseline configuration. Furthermore, the largest changes in the simulated AOD and aerosol distributions were found in high-latitude regions, whereas changes over land where the concentrations, and hence subsequent RF is localized, were smaller. For certain regions and observables, there were notable differences between the baseline and sensitivity simulations. For instance, an improvement in the baseline compared to using the CMIP5 emission inventory was seen for BC surface concentrations, in particular in Asia, while the NMB of AOD compared to AERONET stations in the same region was reduced in the simulation with higher spatial resolution. The importance of using the correct meteorological year was also seen. Such uncertainties will translate to the RFari estimates, along with uncertainties in optical properties such as absorption by organic aerosols and parameterization of BC absorption (Sect. 3.3).

Estimates of radiative impacts depend critically on the confidence in the emission inventories. A detailed discussion of uncertainties in the CEDS inventory is provided by *Hoesly et al.* [2018]. On a global level, the uncertainty in SO₂ emissions tend to be relatively low, although there is an indication of missing SO₂ sources in particular in the Persian Gulf [*McLinden et al.*, 2016], whereas emission factors for BC, OC, NO_x, CO and VOCs have higher uncertainties. Uncertainties in

country-specific emissions can also be much larger, which is particularly true for carbonaceous aerosols. In future CEDS versions, a quantitative uncertainty analysis is planned [Hoesly *et al.*, 2018], which will provide valuable input to modeling studies.

Our study does not include anthropogenic dust, i.e., wind-blown dust from soils disturbed by human activities such as land use practices, deforestation and agriculture, and fugitive combustion and industrial dust from urban sources. These sources could contribute an important fraction of emissions and ambient PM_{2.5} concentrations in some regions [Paul *et al.*, 2012; Sajeed *et al.*, 2017], but are missing from most models today. For instance, a recent study found a 2–16 mg m⁻³ increase in PM_{2.5} concentrations in East and South Asia from anthropogenic fugitive, combustion, and industrial dust emissions. However, the transport processes and optical properties, and hence, radiative impact, is poorly known. We also do not include the effect of aerosol-cloud interactions, which are crucial for the net climate impact of aerosols. For instance, recent studies suggest that the impact of BC on global temperature response is small due to largely compensating direct and rapid adjustment effects [Samset and Myhre, 2015; Stjern *et al.*, 2017]. The composition and distribution of aerosols and oxidants in the pre-industrial atmosphere is uncertain and poorly constrained by observations. However, while this is an important source of uncertainty in estimates of RF due to aerosol-induced cloud albedo changes, it is less important for RFari because the forcing scales quite linearly with aerosol burden [Carslaw *et al.*, 2017].

5 Conclusions

In this study, we have documented the third generation of the Oslo chemical transport model (OsloCTM3) and evaluated the simulated distributions of aerosols, including results from a range of simulations to investigate the sensitivity to uncertainties in scavenging processes, input of emissions and meteorological data and resolution. We have then used the new historical CEDS emission inventory (version 2016; CEDSv16), which will also be used in the upcoming CMIP6, to simulate the temporal evolution of atmospheric concentrations of anthropogenic aerosols, and quantified the temporal evolution of the subsequent radiative forcing due to aerosol-radiation interactions (RFari).

The total AOD from the OsloCTM3 is in good agreement with observations from the AERONET network with a correlation of 0.82 and a normalized mean bias (NMB) of -11.8%. Regionally, the underestimation of observed AOD is higher for stations in China and India than in Europe and North America, as also reflected from the comparison against measured aerosol surface concentrations. High correlations 0.80-0.90 are also found for surface concentrations of BC, OC, sulfate and nitrate aerosols compared with all measurements across Europe, North America and Asia. The corresponding NMB range from -23% for BC and nitrate to -46% and -52% for OC and sulfate, respectively. The OsloCTM3 performs notably better than its predecessor OsloCTM2 in

terms of high-altitude BC distribution as compared with observed BC concentration profiles over the Pacific Ocean from the HIPPO3 campaign. In contrast, the model continues to underestimate observed surface levels of BC during winter and spring. Compared with other recent estimates of aerosol burdens, the OsloCTM3 generally lies close to or above the mean of other global models.

Increasing or reducing the scavenging efficiency, moving to a finer resolution, and using the wrong meteorological year or a different emission inventory results in changes in the global mean aerosol burdens of up to 65%. The burdens of BC, OC and sulfate are particularly sensitive to a reduced efficiency of removal by large-scale ice clouds; a 10 percentage point reduction increases the global burden by 40%, 65% and 20%, respectively. A corresponding increase in the efficiency gives around 10% lower burdens. A significantly better agreement with BC surface concentrations is found when using the CEDSv16 emission inventory compared with the RCP4.5. Furthermore, a notable reduction in the bias of AOD compared to AERONET observations in Asia is found when increasing the horizontal resolution, while the correlation is reduced when using the wrong meteorological year. However, we find no clear evidence of consistently better model performance across all observables and regions in the sensitivity tests than in the baseline configuration. This may in part be influenced by the geographical coverage of observations, as the largest differences in concentrations and AOD from the baseline is found at high altitudes and latitudes where the availability of constraining measurements is limited.

Using the CEDSv16 historical emission inventory we estimate a total net R_{Fari} from all anthropogenic aerosols, relative to 1750, of -0.17 W m^{-2} . This is significantly weaker than the best estimate reported in the IPCC AR5, due to a combination of factors resulting in weaker contributions from both cooling aerosols and BC in our simulations. Our updated R_{Fari} estimate is based on a single global model. As shown by previous studies, there is a large spread estimates of R_{Fari} due to the spread in modeled aerosol distributions. The present analysis shows that uncertainties in emissions, scavenging and optical properties of aerosols can have important impacts on the simulated AOD and subsequent forcing estimates within one model. Additional studies to place our estimates in the context of multi-model spread and provide a comprehensive uncertainty analysis are needed ahead of the IPCC Sixth Assessment Report.

Data availability

The CEDS anthropogenic emissions data is published within the ESGF system <https://esgf-node.llnl.gov/search/input4mips/>. Surface observations used in this study are collected from the following publicly available databases: the EBAS database (<http://ebas.nilu.no/>) hosted by NILU – Norwegian Institute for Air Research. The US national Clean Air Status and Trends monitoring network (CASTNET), available at <http://www.epa.gov/castnet>. The Interagency Monitoring of Protected Visual Environments (IMPROVE), a collaborative association of state, tribal, and federal agencies, and international partners, with the US EPA as the primary funding source and

support from the National Park Service. Data available from <http://vista.cira.colostate.edu/Improve/>. MODIS and MISR AOD retrievals are downloaded from <https://giovanni.gsfc.nasa.gov/giovanni/>. Aircraft measurements from the HIPPO3 flights available from <https://www.eol.ucar.edu/node/524>. Model output available upon request from Marianne T. Lund (m.t.lund@cicero.oslo.no).

Code availability

The OsloCTM3 is stored in a SVN repository at the University of Oslo central subversion system and is available upon request. Please contact m.t.lund@cicero.oslo.no. In this paper, we use the official version 1.0, OsloCTM3v1.0.

Acknowledgements

MTL, GUM, AHS, RBS acknowledges funding from the Norwegian Research Council through grants 250573 (SUPER) and 248834 (QUISARC). The National Center for Atmospheric Research (NCAR) is sponsored by the National Science Foundation (NSF). We would like to express our thanks to all those who are involved in AERONET, IMPROVE, CASTNET, EMEP and ACTRIS measurements efforts and have contributed through operating sites, performing chemical analysis and by submissions of data to public data bases. The authors also acknowledge funding of the Horizon 2020 research and innovation programme ACTRIS-2 Integrating Activities (IA) (grant agreement No 654109). We also acknowledge the Research Council of Norway's programme for supercomputing (NOTUR). The AeroCom database is maintained through basic funding from the Norwegian Meteorological Institute.

Competing interests

The authors declare that they have no conflict of interest.

References

Aiken, A. C., P. F. DeCarlo, J. H. Kroll, D. R. Worsnop, J. A. Huffman, K. S. Docherty, I. M. Ulbrich, C. Mohr, J. R. Kimmel, D. Sueper, Y. Sun, Q. Zhang, A. Trimborn, M. Northway, P. J. Ziemann, M. R. Canagaratna, T. B. Onasch, M. R. Alfarra, A. S. H. Prevot, J. Dommen, J. Duplissy, A. Metzger, U. Baltensperger, and J. L. Jimenez: O/C and OM/OC Ratios of Primary, Secondary, and Ambient Organic Aerosols with High-Resolution Time-of-Flight Aerosol Mass Spectrometry, *Environmental Science & Technology*, 42(12), 4478-4485, doi:10.1021/es703009q, **2008**

963
 964 Amann, M., I. Bertok, J. Borken-Kleefeld, J. Cofala, C. Heyes, L. Höglund-Isaksson, Z. Klimont, B. Nguyen,
 965 M. Posch, P. Rafaj, R. Sandler, W. Schöpp, F. Wagner, and W. Winiwarter: Cost-effective control of air
 966 quality and greenhouse gases in Europe: Modeling and policy applications, *Environmental Modelling &*
 967 *Software*, 26(12), 1489-1501, doi:<http://dx.doi.org/10.1016/j.envsoft.2011.07.012>, **2011**

968
 969 Berglen, T. F., T. K. Berntsen, I. S. A. Isaksen, and J. K. Sundet: A global model of the coupled
 970 sulfur/oxidant chemistry in the troposphere: The sulfur cycle, *Journal of Geophysical Research-*
 971 *Atmospheres*, 109(D19), doi:10.1029/2003jd003948, **2004**

972
 973 Berntsen, T., J. Fuglestad, G. Myhre, F. Stordal, and T. F. Berglen: Abatement of greenhouse gases:
 974 Does location matter?, *Climatic Change*, 74(4), 377-411, doi:10.1007/s10584-006-0433-4, **2006**

975
 976 Bian, H., M. Chin, D. A. Hauglustaine, M. Schulz, G. Myhre, S. E. Bauer, M. T. Lund, V. A. Karydis, T. L.
 977 Kucsera, X. Pan, A. Pozzer, R. B. Skeie, S. D. Steenrod, K. Sudo, K. Tsigaridis, A. P. Tsimpidi, and S. G.
 978 Tsyro: Investigation of global particulate nitrate from the AeroCom Phase III experiment, *Atmos. Chem.*
 979 *Phys.*, 2017(17), 12911-12940, doi:<https://doi.org/10.5194/acp-17-12911-2017>, **2017**

980
 981 Bond, T. C., and R. W. Bergstrom: Light absorption by carbonaceous particles: An investigative review,
 982 *Aerosol Science and Technology*, 40(1), 27-67, doi:10.1080/02786820500421521, **2006**

983
 984 Bond, T. C., S. J. Doherty, D. W. Fahey, P. M. Forster, T. Berntsen, B. J. DeAngelo, M. G. Flanner, S. Ghan,
 985 B. Kärcher, D. Koch, S. Kinne, Y. Kondo, P. K. Quinn, M. C. Sarofim, M. G. Schultz, M. Schulz, C.
 986 Venkataraman, H. Zhang, S. Zhang, N. Bellouin, S. K. Guttikunda, P. K. Hopke, M. Z. Jacobson, J. W.
 987 Kaiser, Z. Klimont, U. Lohmann, J. P. Schwarz, D. Shindell, T. Storelvmo, S. G. Warren, and C. S. Zender:
 988 Bounding the role of black carbon in the climate system: A scientific assessment, *Journal of Geophysical*
 989 *Research: Atmospheres*, 118(11), 5380-5552, doi:10.1002/jgrd.50171, **2013**

990
 991 Boucher, O., D. Randall, P. Artaxo, C. Bretherton, G. Feingold, P. Forster, K. V.-M., Y. Kondo, H. Liao, U.
 992 Lohmann, P. Rasch, S. K. Satheesh, S. Sherwood, B. Stevens, and X. Y. Zhang Clouds and Aerosols: In:
 993 *Climate Change 2013: The Physical Science Basis. Contribution of Working Group I to the Fifth*
 994 *Assessment Report of the Intergovernmental Panel on Climate Change* [Stocker, T.F., D. Qin, G.-K.
 995 Plattner, M. Tignor, S.K. Allen, J. Boschung, A. Nauels, Y. Xia, V. Bex and P.M. Midgley (eds.)]. Cambridge
 996 University Press, Cambridge, United Kingdom and New York, NY, USA., **2013**

997
 998 Bourgeois, Q., and I. Bey: Pollution transport efficiency toward the Arctic: Sensitivity to aerosol
 999 scavenging and source regions, *Journal of Geophysical Research: Atmospheres*, 116(D8), n/a-n/a,
 1000 doi:10.1029/2010JD015096, **2011**

1001
 1002 Browse, J., K. S. Carslaw, S. R. Arnold, K. Pringle, and O. Boucher: The scavenging processes controlling
 1003 the seasonal cycle in Arctic sulphate and black carbon aerosol, *Atmospheric Chemistry and Physics*,
 1004 12(15), 6775-6798, doi:10.5194/acp-12-6775-2012, **2012**

1005
1006 Carslaw, K. S., H. Gordon, D. S. Hamilton, J. S. Johnson, L. A. Regayre, M. Yoshioka, and K. J. Pringle:
1007 Aerosols in the Pre-industrial Atmosphere, *Current Climate Change Reports*, 3(1), 1-15,
1008 doi:10.1007/s40641-017-0061-2, **2017**

1009
1010 Cavalli, F., A. Alastuey, H. Areskoug, D. Ceburnis, J. Čech, J. Genberg, R. M. Harrison, J. L. Jaffrezo, G. Kiss,
1011 P. Laj, N. Mihalopoulos, N. Perez, P. Quincey, J. Schwarz, K. Sellegri, G. Spindler, E. Swietlicki, C.
1012 Theodosi, K. E. Yttri, W. Aas, and J. P. Putaud: A European aerosol phenomenology -4: Harmonized
1013 concentrations of carbonaceous aerosol at 10 regional background sites across Europe, *Atmospheric*
1014 *Environment*, 144, 133-145, doi:<https://doi.org/10.1016/j.atmosenv.2016.07.050>, **2016**

1015
1016 Cooke, W. F., C. Liousse, H. Cachier, and J. Feichter: Construction of a 1 degrees x 1 degrees fossil fuel
1017 emission data set for carbonaceous aerosol and implementation and radiative impact in the ECHAM4
1018 model, *Journal of Geophysical Research-Atmospheres*, 104(D18), 22137-22162,
1019 doi:10.1029/1999jd900187, **1999**

1020
1021 Dubovik, O., and M. D. King: A flexible inversion algorithm for retrieval of aerosol optical properties from
1022 Sun and sky radiance measurements, *Journal of Geophysical Research: Atmospheres*, 105(D16), 20673-
1023 20696, doi:10.1029/2000JD900282, **2000**

1024
1025 Eckhardt, S., B. Quennehen, D. J. L. Olivié, T. K. Berntsen, R. Cherian, J. H. Christensen, W. Collins, S.
1026 Crepinsek, N. Daskalakis, M. Flanner, A. Herber, C. Heyes, Ø. Hodnebrog, L. Huang, M. Kanakidou, Z.
1027 Klimont, J. Langner, K. S. Law, M. T. Lund, R. Mahmood, A. Massling, S. Myriokefalitakis, I. E. Nielsen, J. K.
1028 Nøjgaard, J. Quaas, P. K. Quinn, J. C. Raut, S. T. Rumbold, M. Schulz, S. Sharma, R. B. Skeie, H. Skov, T.
1029 Uttal, K. von Salzen, and A. Stohl: Current model capabilities for simulating black carbon and sulfate
1030 concentrations in the Arctic atmosphere: a multi-model evaluation using a comprehensive measurement
1031 data set, *Atmos. Chem. Phys.*, 15(16), 9413-9433, doi:10.5194/acp-15-9413-2015, **2015**

1032
1033 Fan, S. M., J. P. Schwarz, J. Liu, D. W. Fahey, P. Ginoux, L. W. Horowitz, H. Levy, Y. Ming, and J. R.
1034 Spackman: Inferring ice formation processes from global-scale black carbon profiles observed in the
1035 remote atmosphere and model simulations, *Journal of Geophysical Research: Atmospheres*, 117(D23),
1036 D23205, doi:10.1029/2012JD018126, **2012**

1037
1038 Feng, Y., V. Ramanathan, and V. R. Kotamarthi: Brown carbon: a significant atmospheric absorber of
1039 solar radiation?, *Atmos. Chem. Phys.*, 13(17), 8607-8621, doi:10.5194/acp-13-8607-2013, **2013**

1040
1041 Gantt, B., M. S. Johnson, M. Crippa, A. S. H. Prévôt, and N. Meskhidze: Implementing marine organic
1042 aerosols into the GEOS-Chem model, *Geosci. Model Dev.*, 8(3), 619-629, doi:10.5194/gmd-8-619-2015,
1043 **2015**

1044
1045 Granier, C., B. Bessagnet, T. Bond, A. D'Angiola, H. Denier van der Gon, G. J. Frost, A. Heil, J. W. Kaiser, S.
1046 Kinne, Z. Klimont, S. Kloster, J.-F. Lamarque, C. Liousse, T. Masui, F. Meleux, A. Mieville, T. Ohara, J.-C.
1047 Raut, K. Riahi, M. G. Schultz, S. J. Smith, A. Thompson, J. van Aardenne, G. R. van der Werf, and D. P. van

1048 Vuuren: Evolution of anthropogenic and biomass burning emissions of air pollutants at global and
 1049 regional scales during the 1980–2010 period, *Climatic Change*, 109(1), 163, doi:10.1007/s10584-011-
 1050 0154-1, **2011**

1051

1052 Grini, A., G. Myhre, J. K. Sundet, and I. S. A. Isaksen: Modeling the annual cycle of sea salt in the global
 1053 3D model Oslo CTM2: Concentrations, fluxes, and radiative impact, *Journal of Climate*, 15(13), 1717-
 1054 1730, doi:10.1175/1520-0442(2002)015<1717:mtacos>2.0.co;2, **2002**

1055

1056 Grini, A., G. Myhre, C. S. Zender, and I. S. A. Isaksen: Model simulations of dust sources and transport in
 1057 the global atmosphere: Effects of soil erodibility and wind speed variability, *Journal of Geophysical*
 1058 *Research-Atmospheres*, 110(D2), doi:10.1029/2004jd005037, **2005**

1059

1060 Hodnebrog, Ø., G. Myhre, and B. H. Samset: How shorter black carbon lifetime alters its climate effect,
 1061 *Nat Commun*, 5, 5065, doi:10.1038/ncomms6065, **2014**

1062

1063 Hoesly, R. M., S. J. Smith, L. Feng, Z. Klimont, G. Janssens-Maenhout, T. Pitkanen, J. J. Seibert, L. Vu, R. J.
 1064 Andres, R. M. Bolt, T. C. Bond, L. Dawidowski, N. Kholod, J. I. Kurokawa, M. Li, L. Liu, Z. Lu, M. C. P.
 1065 Moura, P. R. O'Rourke, and Q. Zhang: Historical (1750–2014) anthropogenic emissions of reactive gases
 1066 and aerosols from the Community Emission Data System (CEDS), *Geosci. Model Dev.*, 2018(11), 369-408,
 1067 doi:<https://doi.org/10.5194/gmd-11-369-2018>, **2018**

1068

1069 Holben, B. N., T. F. Eck, I. Slutsker, D. Tanré, J. P. Buis, A. Setzer, E. Vermote, J. A. Reagan, Y. J. Kaufman,
 1070 T. Nakajima, F. Lavenue, I. Jankowiak, and A. Smirnov: AERONET—A Federated Instrument Network and
 1071 Data Archive for Aerosol Characterization, *Remote Sensing of Environment*, 66(1), 1-16,
 1072 doi:[https://doi.org/10.1016/S0034-4257\(98\)00031-5](https://doi.org/10.1016/S0034-4257(98)00031-5), **1998**

1073

1074 Hoyle, C. R., T. Berntsen, G. Myhre, and I. S. A. Isaksen: Secondary organic aerosol in the global aerosol-
 1075 chemical transport model Oslo CTM2, *Atmos. Chem. Phys.*, 7(5675-5694), **2007**

1076

1077 Jaeglé, L., P. K. Quinn, T. S. Bates, B. Alexander, and J. T. Lin: Global distribution of sea salt aerosols: new
 1078 constraints from in situ and remote sensing observations, *Atmos. Chem. Phys.*, 11(7), 3137-3157,
 1079 doi:10.5194/acp-11-3137-2011, **2011**

1080

1081 Kinne, S., D. O'Donnell, P. Stier, S. Kloster, K. Zhang, H. Schmidt, S. Rast, M. Giorgetta, T. F. Eck, and B.
 1082 Stevens: MAC-v1: A new global aerosol climatology for climate studies, *J. Adv. Model. Earth Syst.*, 5, 704-
 1083 740, doi:doi:10.1002/jame.20035, **2013**

1084

1085 Kipling, Z., P. Stier, C. E. Johnson, G. W. Mann, N. Bellouin, S. E. Bauer, T. Bergman, M. Chin, T. Diehl, S. J.
 1086 Ghan, T. Iversen, A. Kirkevåg, H. Kokkola, X. Liu, G. Luo, T. van Noije, K. J. Pringle, K. von Salzen, M.
 1087 Schulz, Ø. Seland, R. B. Skeie, T. Takemura, K. Tsigaridis, and K. Zhang: What controls the vertical
 1088 distribution of aerosol? Relationships between process sensitivity in HadGEM3–UKCA and inter-model

1089 variation from AeroCom Phase II, *Atmos. Chem. Phys.*, 16(4), 2221-2241, doi:10.5194/acp-16-2221-
1090 2016, **2016**

1091

1092 Kipling, Z., P. Stier, J. P. Schwarz, A. E. Perring, J. R. Spackman, G. W. Mann, C. E. Johnson, and P. J.
1093 Telford: Constraints on aerosol processes in climate models from vertically-resolved aircraft
1094 observations of black carbon, *Atmos. Chem. Phys.*, 13(12), 5969-5986, doi:10.5194/acp-13-5969-2013,
1095 **2013**

1096

1097 Kirchstetter, T. W., T. Novakov, and P. V. Hobbs: Evidence that the spectral dependence of light
1098 absorption by aerosols is affected by organic carbon, *Journal of Geophysical Research: Atmospheres*,
1099 109(D21), n/a-n/a, doi:10.1029/2004JD004999, **2004**

1100

1101 Klimont, Z., K. Kupiainen, C. Heyes, P. Purohit, J. Cofala, P. Rafaj, J. Borken-Kleefeld, and W. Schöpp:
1102 Global anthropogenic emissions of particulate matter including black carbon, *Atmos. Chem. Phys.*,
1103 17(14), 8681-8723, doi:10.5194/acp-17-8681-2017, **2017**

1104

1105 Klimont, Z., S. J. Smith, and J. Cofala: The last decade of global anthropogenic sulfur dioxide: 2000–2011
1106 emissions, *Environmental Research Letters*, 8(1), 014003, **2013**

1107

1108 Kumar, R., M. C. Barth, G. G. Pfister, V. S. Nair, S. D. Ghude, and N. Ojha: What controls the seasonal
1109 cycle of black carbon aerosols in India?, *Journal of Geophysical Research: Atmospheres*, 120(15), 7788-
1110 7812, doi:10.1002/2015JD023298, **2015**

1111

1112 Lamarque, J. F., T. C. Bond, V. Eyring, C. Granier, A. Heil, Z. Klimont, D. Lee, C. Liousse, A. Mieville, B.
1113 Owen, M. G. Schultz, D. Shindell, S. J. Smith, E. Stehfest, J. Van Aardenne, O. R. Cooper, M. Kainuma, N.
1114 Mahowald, J. R. McConnell, V. Naik, K. Riahi, and D. P. van Vuuren: Historical (1850–2000) gridded
1115 anthropogenic and biomass burning emissions of reactive gases and aerosols: methodology and
1116 application, *Atmos. Chem. Phys.*, 10(15), 7017-7039, doi:10.5194/acp-10-7017-2010, **2010**

1117

1118 Lavery, T. F., C. M. Rogers, R. Baumgardner, and K. P. Mishoe: Intercomparison of Clean Air Status and
1119 Trends Network Nitrate and Nitric Acid Measurements with Data from Other Monitoring Programs,
1120 *Journal of the Air & Waste Management Association*, 59(2), 214-226, doi:10.3155/1047-3289.59.2.214,
1121 **2009**

1122

1123 Lee, Y. H., J. F. Lamarque, M. G. Flanner, C. Jiao, D. T. Shindell, T. Berntsen, M. M. Bisiaux, J. Cao, W. J.
1124 Collins, M. Curran, R. Edwards, G. Faluvegi, S. Ghan, L. W. Horowitz, J. R. McConnell, J. Ming, G. Myhre,
1125 T. Nagashima, V. Naik, S. T. Rumbold, R. B. Skeie, K. Sudo, T. Takemura, F. Thevenon, B. Xu, and J. H.
1126 Yoon: Evaluation of preindustrial to present-day black carbon and its albedo forcing from Atmospheric
1127 Chemistry and Climate Model Intercomparison Project (ACCMIP), *Atmospheric Chemistry and Physics*,
1128 13(5), 2607-2634, doi:10.5194/acp-13-2607-2013, **2013**

1129

1130 Li, C., C. McLinden, V. Fioletov, N. Krotkov, S. Carn, J. Joiner, D. Streets, H. He, X. Ren, Z. Li, and R. R.
 1131 Dickerson: India Is Overtaking China as the World's Largest Emitter of Anthropogenic Sulfur Dioxide,
 1132 Scientific Reports, 7(1), 14304, doi:10.1038/s41598-017-14639-8, **2017**
 1133
 1134 Lund, M. T., and T. Berntsen: Parameterization of black carbon aging in the OsloCTM2 and implications
 1135 for regional transport to the Arctic, Atmos. Chem. Phys., 12(15), 6999-7014, doi:10.5194/acp-12-6999-
 1136 2012, **2012**
 1137
 1138 Lund, M. T., T. K. Berntsen, and B. H. Samset: Sensitivity of black carbon concentrations and climate
 1139 impact to aging and scavenging in OsloCTM2–M7, Atmos. Chem. Phys., 17(9), 6003-6022,
 1140 doi:10.5194/acp-17-6003-2017, **2017**
 1141
 1142 Lund, M. T., B. H. Samset, R. B. Skeie, D. Watson-Parris, J. M. Katich, J. P. Schwarz, and B. Weinzierl:
 1143 Short Black Carbon lifetime inferred from a global set of aircraft observations. Accepted manuscript. ,
 1144 npj Climate and Atmospheric Science 1, 31, doi:10.1038/s41612-018-0040-x, **2018**
 1145
 1146 Mahmood, R., K. von Salzen, M. Flanner, M. Sand, J. Langner, H. Wang, and L. Huang: Seasonality of
 1147 global and Arctic black carbon processes in the Arctic Monitoring and Assessment Programme models,
 1148 Journal of Geophysical Research: Atmospheres, 121(12), 7100-7116, doi:10.1002/2016JD024849, **2016**
 1149
 1150 McLinden, C. A., V. Fioletov, M. W. Shephard, N. Krotkov, C. Li, R. V. Martin, M. D. Moran, and J. Joiner:
 1151 Space-based detection of missing sulfur dioxide sources of global air pollution, Nature Geoscience, 9,
 1152 496, doi:10.1038/ngeo2724
 1153 <https://www.nature.com/articles/ngeo2724#supplementary-information>, **2016**
 1154
 1155 Metzger, S., F. Dentener, M. Krol, A. Jeuken, and J. Lelieveld: Gas/aerosol partitioning - 2. Global
 1156 modeling results, Journal of Geophysical Research-Atmospheres, 107(D16), doi:10.1029/2001jd001103,
 1157 **2002a**
 1158
 1159 Metzger, S., F. Dentener, S. Pandis, and J. Lelieveld: Gas/aerosol partitioning: 1. A computationally
 1160 efficient model, Journal of Geophysical Research-Atmospheres, 107(D16), doi:10.1029/2001jd001102,
 1161 **2002b**
 1162
 1163 MISR (2018), Data product specification for the MISR level 2 aerosol product, Garay, M.J., et al.,
 1164 https://eosweb.larc.nasa.gov/project/misr/DPS_AEROSOL_V023.20180125.pdf (accessed 04/26/2018),
 1165 edited.
 1166 MOD08: MODIS Level 3 Atmosphere Products (MOD 08), Data Products Handbook Volume 2.
 1167 https://modis.gsfc.nasa.gov/data/dataproduct/dataproducts.php?MOD_NUMBER=08 (accessed
 1168 04/26/2018), **2018**
 1169
 1170 Myhre, G., W. Aas, R. Cherian, W. Collins, G. Faluvegi, M. Flanner, P. Forster, Ø. Hodnebrog, Z. Klimont,
 1171 M. T. Lund, J. Mülmenstädt, C. Lund Myhre, D. Olivie, M. Prather, J. Quaas, B. H. Samset, J. L. Schnell, M.

1172 Schulz, D. Shindell, R. B. Skeie, T. Takemura, and S. Tsyro: Multi-model simulations of aerosol and ozone
 1173 radiative forcing due to anthropogenic emission changes during the period 1990–2015, *Atmos. Chem.*
 1174 *Phys.*, 17(4), 2709–2720, doi:10.5194/acp-17-2709-2017, **2017**

1175
 1176 Myhre, G., N. Bellouin, T. F. Berglen, T. K. Berntsen, O. Boucher, A. L. F. Grini, I. S. A. Isaksen, M.
 1177 Johnsrud, M. I. Mishchenko, F. Stordal, and D. Tanré: Comparison of the radiative properties and direct
 1178 radiative effect of aerosols from a global aerosol model and remote sensing data over ocean, *Tellus B*,
 1179 59(1), 115–129, doi:10.1111/j.1600-0889.2006.00226.x, **2007**

1180
 1181 Myhre, G., T. F. Berglen, M. Johnsrud, C. R. Hoyle, T. K. Berntsen, S. A. Christopher, D. W. Fahey, I. S. A.
 1182 Isaksen, T. A. Jones, R. A. Kahn, N. Loeb, P. Quinn, L. Remer, J. P. Schwarz, and K. E. Yttri: Modelled
 1183 radiative forcing of the direct aerosol effect with multi-observation evaluation, *Atmospheric Chemistry*
 1184 *and Physics*, 9(4), 1365–1392, doi:10.5194/acp-9-1365-2009, **2009**

1185
 1186 Myhre, G., A. Grini, and S. Metzger: Modelling of nitrate and ammonium-containing aerosols in presence
 1187 of sea salt, *Atmos. Chem. Phys.*, 6, 4809–4821, **2006**

1188
 1189 Myhre, G., B. H. Samset, M. Schulz, Y. Balkanski, S. Bauer, T. K. Berntsen, H. Bian, N. Bellouin, M. Chin, T.
 1190 Diehl, R. C. Easter, J. Feichter, S. J. Ghan, D. Hauglustaine, T. Iversen, S. Kinne, A. Kirkevåg, J. F.
 1191 Lamarque, G. Lin, X. Liu, M. T. Lund, G. Luo, X. Ma, T. van Noije, J. E. Penner, P. J. Rasch, A. Ruiz, Ø.
 1192 Seland, R. B. Skeie, P. Stier, T. Takemura, K. Tsigaridis, P. Wang, Z. Wang, L. Xu, H. Yu, F. Yu, J. H. Yoon, K.
 1193 Zhang, H. Zhang, and C. Zhou: Radiative forcing of the direct aerosol effect from AeroCom Phase II
 1194 simulations, *Atmos. Chem. Phys.*, 13(4), 1853–1877, doi:10.5194/acp-13-1853-2013, **2013a**

1195
 1196 Myhre, G., D. Shindell, F.-M. Brèon, W. Collins, J. Fuglestad, J. Huang, D. Koch, J.-F. Lamarque, D. Lee,
 1197 B. Mendoza, T. Nakajima, A. Robock, G. Stephens, T. Takemura, and H. Zhang: Anthropogenic and
 1198 natural radiative forcing. In: *Climate Change 2013: The Physical Science Basis. Contribution of Working*
 1199 *Group I to the Fifth Assessment Report of the Intergovernmental Panel on Climate Change* [Stocker, T.F.,
 1200 D., Qin, G.-K. Plattner, M. Tignor, S.K. Allen, J. Boschung, A. Nauels, Y. Xia, V. Bex and P.M. Midgley (eds).
 1201 Cambridge University Press, Cambridge, United Kingdom and New York, NY, USA **2013b**

1202
 1203 Neu, J. L., and M. J. Prather: Toward a more physical representation of precipitation scavenging in global
 1204 chemistry models: cloud overlap and ice physics and their impact on tropospheric ozone, *Atmos. Chem.*
 1205 *Phys.*, 12(7), 3289–3310, doi:10.5194/acp-12-3289-2012, **2012**

1206
 1207 Parhi, P., A. Giannini, P. Gentile, and U. Lall: Resolving Contrasting Regional Rainfall Responses to El
 1208 Niño over Tropical Africa, *Journal of Climate*, 29(4), 1461–1476, doi:10.1175/jcli-d-15-0071.1, **2016**

1209
 1210 Paul, G., P. J. M., G. T. E., H. N. Christina, and Z. Ming: Global - scale attribution of anthropogenic and
 1211 natural dust sources and their emission rates based on MODIS Deep Blue aerosol products, *Reviews of*
 1212 *Geophysics*, 50(3), doi:doi:10.1029/2012RG000388, **2012**

1213

1214 Petzold, A., J. A. Ogren, M. Fiebig, P. Laj, S. M. Li, U. Baltensperger, T. Holzer-Popp, S. Kinne, G.
 1215 Pappalardo, N. Sugimoto, C. Wehrli, A. Wiedensohler, and X. Y. Zhang: Recommendations for reporting
 1216 "black carbon" measurements, *Atmos. Chem. Phys.*, 13(16), 8365-8379, doi:10.5194/acp-13-8365-2013,
 1217 **2013**

1218

1219 Putaud, J. P., R. Van Dingenen, A. Alastuey, H. Bauer, W. Birmili, J. Cyrys, H. Flentje, S. Fuzzi, R. Gehrig, H.
 1220 C. Hansson, R. M. Harrison, H. Herrmann, R. Hitzenberger, C. Hüglin, A. M. Jones, A. Kasper-Giebl, G.
 1221 Kiss, A. Kousa, T. A. J. Kuhlbusch, G. Löschau, W. Maenhaut, A. Molnar, T. Moreno, J. Pekkanen, C.
 1222 Perrino, M. Pitz, H. Puxbaum, X. Querol, S. Rodriguez, I. Salma, J. Schwarz, J. Smolik, J. Schneider, G.
 1223 Spindler, H. ten Brink, J. Tursic, M. Viana, A. Wiedensohler, and F. Raes: A European aerosol
 1224 phenomenology – 3: Physical and chemical characteristics of particulate matter from 60 rural, urban,
 1225 and kerbside sites across Europe, *Atmospheric Environment*, 44(10), 1308-1320,
 1226 doi:<https://doi.org/10.1016/j.atmosenv.2009.12.011>, **2010**

1227

1228 Randerson, J. T., G. R. van der Werf, L. Giglio, G. J. Collatz, and P. S. Kasibhatla: Global Fire Emissions
 1229 Database, Version 4.1 (GFEDv4). ORNL DAAC, Oak Ridge, Tennessee, USA. ,
 1230 doi:<https://doi.org/10.3334/ORNLDAAAC/1293>, **2017**

1231

1232 Sajeev, P., V. M. Randall, S. Graydon, L. W. Crystal, D. Aaron van, B. Michael, K. H. Daven, K. Zbigniew, V.
 1233 Chandra, K. G. Sarath, and Z. Qiang: Anthropogenic fugitive, combustion and industrial dust is a
 1234 significant, underrepresented fine particulate matter source in global atmospheric models,
 1235 *Environmental Research Letters*, 12(4), 044018, **2017**

1236

1237 Samset, B. H., and G. Myhre: Climate response to externally mixed black carbon as a function of altitude,
 1238 *Journal of Geophysical Research: Atmospheres*, 120(7), 2913-2927, doi:10.1002/2014JD022849, **2015**

1239

1240 Samset, B. H., G. Myhre, A. Herber, Y. Kondo, S. M. Li, N. Moteki, M. Koike, N. Oshima, J. P. Schwarz, Y.
 1241 Balkanski, S. E. Bauer, N. Bellouin, T. K. Berntsen, H. Bian, M. Chin, T. Diehl, R. C. Easter, S. J. Ghan, T.
 1242 Iversen, A. Kirkevåg, J. F. Lamarque, G. Lin, X. Liu, J. E. Penner, M. Schulz, Ø. Seland, R. B. Skeie, P. Stier,
 1243 T. Takemura, K. Tsigaridis, and K. Zhang: Modelled black carbon radiative forcing and atmospheric
 1244 lifetime in AeroCom Phase II constrained by aircraft observations, *Atmos. Chem. Phys.*, 14(22), 12465-
 1245 12477, doi:10.5194/acp-14-12465-2014, **2014**

1246

1247 Samset, B. H., G. Myhre, M. Schulz, Y. Balkanski, S. Bauer, T. K. Berntsen, H. Bian, N. Bellouin, T. Diehl, R.
 1248 C. Easter, S. J. Ghan, T. Iversen, S. Kinne, A. Kirkevåg, J. F. Lamarque, G. Lin, X. Liu, J. E. Penner, Ø. Seland,
 1249 R. B. Skeie, P. Stier, T. Takemura, K. Tsigaridis, and K. Zhang: Black carbon vertical profiles strongly affect
 1250 its radiative forcing uncertainty, *Atmos. Chem. Phys.*, 13(5), 2423-2434, doi:10.5194/acp-13-2423-2013,
 1251 **2013**

1252

1253 Samset, B. H., C. W. Stjern, E. Andrews, R. A. Kahn, G. Myhre, M. Schulz, and G. L. Schuster: Aerosol
 1254 Absorption: Progress Towards Global and Regional Constraints, *Current Climate Change Reports*,
 1255 doi:10.1007/s40641-018-0091-4, **2018**

1256

1257 Sato, Y., H. Miura, H. Yashiro, D. Goto, T. Takemura, H. Tomita, and T. Nakajima: Unrealistically pristine
 1258 air in the Arctic produced by current global scale models, *Scientific Reports*, 6, 26561,
 1259 doi:10.1038/srep26561

1260 <http://www.nature.com/articles/srep26561#supplementary-information>, **2016**

1261

1262 Schutgens, N., S. Tsyro, E. Gryspeerd, D. Goto, N. Weigum, M. Schulz, and P. Stier: On the spatio-
 1263 temporal representativeness of observations, *Atmos. Chem. Phys.*, 17(16), 9761-9780, doi:10.5194/acp-
 1264 17-9761-2017, **2017**

1265

1266 Schutgens, N. A. J., E. Gryspeerd, N. Weigum, S. Tsyro, D. Goto, M. Schulz, and P. Stier: Will a perfect
 1267 model agree with perfect observations? The impact of spatial sampling, *Atmos. Chem. Phys.*, 16(10),
 1268 6335-6353, doi:10.5194/acp-16-6335-2016, **2016a**

1269

1270 Schutgens, N. A. J., D. G. Partridge, and P. Stier: The importance of temporal collocation for the
 1271 evaluation of aerosol models with observations, *Atmos. Chem. Phys.*, 16(2), 1065-1079,
 1272 doi:10.5194/acp-16-1065-2016, **2016b**

1273

1274 Schwarz, J. P., B. H. Samset, A. E. Perring, J. R. Spackman, R. S. Gao, P. Stier, M. Schulz, F. L. Moore, E. A.
 1275 Ray, and D. W. Fahey: Global-scale seasonally resolved black carbon vertical profiles over the Pacific,
 1276 *Geophysical Research Letters*, 40(20), 2013GL057775, doi:10.1002/2013GL057775, **2013**

1277

1278 Sindelarova, K., C. Granier, I. Bouarar, A. Guenther, S. Tilmes, T. Stavrou, J. F. Müller, U. Kuhn, P.
 1279 Stefani, and W. Knorr: Global data set of biogenic VOC emissions calculated by the MEGAN model over
 1280 the last 30 years, *Atmos. Chem. Phys.*, 14(17), 9317-9341, doi:10.5194/acp-14-9317-2014, **2014**

1281

1282 Skeie, R. B., T. Berntsen, G. Myhre, C. A. Pedersen, J. Ström, S. Gerland, and J. A. Ogren: Black carbon in
 1283 the atmosphere and snow, from pre-industrial times until present, *Atmospheric Chemistry and Physics*,
 1284 11(14), 6809-6836, doi:10.5194/acp-11-6809-2011, **2011**

1285

1286 Smith, S. J., Y. Zhou, P. Kyle, H. Wang, and H. Yu: A Community Emissions Data System (CEDS): Emissions
 1287 for CMIP6 and Beyond. , **2015**

1288

1289 Sofiev, M., J. Soares, M. Prank, G. de Leeuw, and J. Kukkonen: A regional-to-global model of emission
 1290 and transport of sea salt particles in the atmosphere, *Journal of Geophysical Research: Atmospheres*,
 1291 116(D21), n/a-n/a, doi:10.1029/2010JD014713, **2011**

1292

1293 Stamnes, K., S. C. Tsay, W. Wiscombe, and K. Jayaweera: Numerically stable algorithm for discrete-
 1294 ordinate-method radiative transfer in multiple scattering and emitting layered media, *Appl. Opt.*, 27(12),
 1295 2502-2509, doi:10.1364/AO.27.002502, **1988**

1296

1297 Stjern, C. W., B. H. Samset, G. Myhre, P. M. Forster, Ø. Hodnebrog, T. Andrews, O. Boucher, G. Faluvegi,
 1298 T. Iversen, M. Kassoar, V. Kharin, A. Kirkevåg, J.-F. Lamarque, D. Olivié, T. Richardson, D. Shawki, D.
 1299 Shindell, C. J. Smith, T. Takemura, and A. Voulgarakis: Rapid Adjustments Cause Weak Surface
 1300 Temperature Response to Increased Black Carbon Concentrations, *Journal of Geophysical Research:*
 1301 *Atmospheres*, 122(21), 11,462-411,481, doi:10.1002/2017JD027326, **2017**
 1302
 1303 Søvde, O. A., M. J. Prather, I. S. A. Isaksen, T. K. Berntsen, F. Stordal, X. Zhu, C. D. Holmes, and J. Hsu: The
 1304 chemical transport model Oslo CTM3, *Geosci. Model Dev.*, 5(6), 1441-1469, doi:10.5194/gmd-5-1441-
 1305 2012, **2012**
 1306
 1307 Taylor, K. E., R. J. Stouffer, and G. A. Meehl: An Overview of CMIP5 and the Experiment Design, *Bulletin*
 1308 *of the American Meteorological Society*, 93(4), 485-498, doi:10.1175/bams-d-11-00094.1, **2012**
 1309
 1310 Thomson, A. M., K. V. Calvin, S. J. Smith, G. P. Kyle, A. Volke, P. Patel, S. Delgado-Arias, B. Bond-
 1311 Lamberty, M. A. Wise, L. E. Clarke, and J. A. Edmonds: RCP4.5: a pathway for stabilization of radiative
 1312 forcing by 2100, *Climatic Change*, 109(1), 77, doi:10.1007/s10584-011-0151-4, **2011**
 1313
 1314 Tsigaridis, K., N. Daskalakis, M. Kanakidou, P. J. Adams, P. Artaxo, R. Bahadur, Y. Balkanski, S. E. Bauer, N.
 1315 Bellouin, A. Benedetti, T. Bergman, T. K. Berntsen, J. P. Beukes, H. Bian, K. S. Carslaw, M. Chin, G. Curci,
 1316 T. Diehl, R. C. Easter, S. J. Ghan, S. L. Gong, A. Hodzic, C. R. Hoyle, T. Iversen, S. Jathar, J. L. Jimenez, J. W.
 1317 Kaiser, A. Kirkevåg, D. Koch, H. Kokkola, Y. H. Lee, G. Lin, X. Liu, G. Luo, X. Ma, G. W. Mann, N.
 1318 Mihalopoulos, J. J. Morcrette, J. F. Müller, G. Myhre, S. Myriokefalitakis, N. L. Ng, D. O'Donnell, J. E.
 1319 Penner, L. Pozzoli, K. J. Pringle, L. M. Russell, M. Schulz, J. Sciare, Ø. Seland, D. T. Shindell, S. Sillman, R. B.
 1320 Skeie, D. Spracklen, T. Stavrakou, S. D. Steenrod, T. Takemura, P. Tiitta, S. Tilmes, H. Tost, T. van Noije, P.
 1321 G. van Zyl, K. von Salzen, F. Yu, Z. Wang, Z. Wang, R. A. Zaveri, H. Zhang, K. Zhang, Q. Zhang, and X.
 1322 Zhang: The AeroCom evaluation and intercomparison of organic aerosol in global models, *Atmos. Chem.*
 1323 *Phys.*, 14(19), 10845-10895, doi:10.5194/acp-14-10845-2014, **2014**
 1324
 1325 Turpin, B. J., and H.-J. Lim: Species Contributions to PM_{2.5} Mass Concentrations: Revisiting Common
 1326 Assumptions for Estimating Organic Mass, *Aerosol Science and Technology*, 35(1), 602-610,
 1327 doi:10.1080/02786820119445, **2001**
 1328
 1329 Tørseth, K., W. Aas, K. Breivik, A. M. Fjæraa, M. Fiebig, A. G. Hjellbrekke, C. Lund Myhre, S. Solberg, and
 1330 K. E. Yttri: Introduction to the European Monitoring and Evaluation Programme (EMEP) and observed
 1331 atmospheric composition change during 1972 - 2009, *Atmos. Chem. Phys.*, 12(12), 5447-5481,
 1332 doi:10.5194/acp-12-5447-2012, **2012**
 1333
 1334 van Marle, M. J. E., S. Kloster, B. I. Magi, J. R. Marlon, A. L. Daniau, R. D. Field, A. Arneth, M. Forrest, S.
 1335 Hantson, N. M. Kehrwald, W. Knorr, G. Lasslop, F. Li, S. Mangeon, C. Yue, J. W. Kaiser, and G. R. van der
 1336 Werf: Historic global biomass burning emissions for CMIP6 (BB4CMIP) based on merging satellite
 1337 observations with proxies and fire models (1750–2015), *Geosci. Model Dev.*, 10(9), 3329-3357,
 1338 doi:10.5194/gmd-10-3329-2017, **2017**
 1339

1340 van Vuuren, D. P., J. Edmonds, M. Kainuma, K. Riahi, A. Thomson, K. Hibbard, G. C. Hurtt, T. Kram, V.
 1341 Krey, J.-F. Lamarque, T. Masui, M. Meinshausen, N. Nakicenovic, S. J. Smith, and S. K. Rose: The
 1342 representative concentration pathways: an overview, *Climatic Change*, 109(1), 5, doi:10.1007/s10584-
 1343 011-0148-z, **2011**

1344
 1345 Wang, R., E. Andrews, Y. Balkanski, O. Boucher, G. Myhre, B. H. Samset, M. Schulz, G. L. Schuster, M.
 1346 Valari, and S. Tao: Spatial Representativeness Error in the Ground-Level Observation Networks for Black
 1347 Carbon Radiation Absorption, *Geophysical Research Letters*, 45, 2106-2114,
 1348 doi:10.1002/2017GL076817, **2018**

1349
 1350 Wang, R., Y. Balkanski, O. Boucher, P. Ciais, G. L. Schuster, F. Chevallier, B. H. Samset, J. Liu, S. Piao, M.
 1351 Valari, and S. Tao: Estimation of global black carbon direct radiative forcing and its uncertainty
 1352 constrained by observations, *Journal of Geophysical Research: Atmospheres*, 121(10), 5948-5971,
 1353 doi:10.1002/2015JD024326, **2016**

1354
 1355 Wang, R., S. Tao, Y. Balkanski, P. Ciais, O. Boucher, J. Liu, S. Piao, H. Shen, M. R. Vuolo, M. Valari, H.
 1356 Chen, Y. Chen, A. Cozic, Y. Huang, B. Li, W. Li, G. Shen, B. Wang, and Y. Zhang: Exposure to ambient black
 1357 carbon derived from a unique inventory and high-resolution model, *Proceedings of the National*
 1358 *Academy of Sciences*, 111(7), 2459-2463, doi:10.1073/pnas.1318763111, **2014**

1359
 1360 Witek, M. L., D. J. Diner, and M. J. Garay: Satellite assessment of sea spray aerosol productivity:
 1361 Southern Ocean case study, *Journal of Geophysical Research: Atmospheres*, 121(2), 872-894,
 1362 doi:10.1002/2015JD023726, **2016**

1363
 1364 Wofsy, S. C., H. S. Team, T. Cooperating Modellers, and T. Satellite: HIAPER Pole-to-Pole Observations
 1365 (HIPPO): fine-grained, global-scale measurements of climatically important atmospheric gases and
 1366 aerosols, *Philosophical Transactions of the Royal Society a-Mathematical Physical and Engineering*
 1367 *Sciences*, 369(1643), 2073-2086, doi:10.1098/rsta.2010.0313, **2011**

1368
 1369 Xie, M., M. D. Hays, and A. L. Holder: Light-absorbing organic carbon from prescribed and laboratory
 1370 biomass burning and gasoline vehicle emissions, *Scientific Reports*, 7(1), 7318, doi:10.1038/s41598-017-
 1371 06981-8, **2017**

1372
 1373 Zanatta, M., M. Gysel, N. Bukowiecki, T. Müller, E. Weingartner, H. Areskoug, M. Fiebig, K. E. Yttri, N.
 1374 Mihalopoulos, G. Kouvarakis, D. Beddows, R. M. Harrison, F. Cavalli, J. P. Putaud, G. Spindler, A.
 1375 Wiedensohler, A. Alastuey, M. Pandolfi, K. Sellegri, E. Swietlicki, J. L. Jaffrezo, U. Baltensperger, and P.
 1376 Laj: A European aerosol phenomenology-5: Climatology of black carbon optical properties at 9 regional
 1377 background sites across Europe, *Atmospheric Environment*, 145, 346-364,
 1378 doi:<https://doi.org/10.1016/j.atmosenv.2016.09.035>, **2016**

1379
 1380 Zender, C. S., H. Bian, and D. Newman: Mineral Dust Entrainment and Deposition (DEAD) model:
 1381 Description and 1990s dust climatology, *Journal of Geophysical Research: Atmospheres*, 108(D14),
 1382 doi:10.1029/2002JD002775, **2003**

Zhang, X. Y., Y. Q. Wang, T. Niu, X. C. Zhang, S. L. Gong, Y. M. Zhang , and J. Y. Sun: Atmospheric aerosol compositions in China: spatial/temporal variability, chemical signature, regional haze distribution and comparison with global models. , Atmos. Chem. Phys., 12, 779-799, **2012**

Tables

Table 1: Summary and description of simulations in this study

Name	Athropogenic emissions	Year	Res	Description
CEDSv16/CMIP6	CEDS, version released in 2016	2010	2x2	Baseline simulation, 2.25x2.25 degree resolution
ECLv5	ECLIPSEv5	2010	2x2	As baseline, but with ECLIPSEv5 emissions
RCP/CMIP5	RCP4.5	2010	2x2	As baseline, but RCP4.5/CMIP5 emissions
LSIDEC	CEDS	2010	2x2	Reduced scavenging of all aerosols by large-scale ice clouds
LSIINC	CEDS	2010	2x2	Increased scavenging of all aerosols by large-scale ice clouds
SOLDEC	CEDS	2010	2x2	Decreased scavenging of all aerosols by convective and large-scale liquid precipitation
1x1RES	CEDS	2010	1x1	Same as baseline, but on 1.125x1.125 degree resolution
METDTA	CEDS	2010	2x2	Year 2010 emissions, but 2000 meteorology
Historical	CEDS/	1750-2014	2x2	Time-slice simulations for year 1750, 1850, 1900, 1910, 1920, 1930, 1940, 1950, 1960, 1970, 1980, 1985, 1990, 1995, 2000, 2005, 2010, 2014

Table 2: Fraction of aerosol mass available for wet scavenging by convective, large-scale liquid and large-scale ice precipitation in baseline setup and in the three sensitivity tests. Phil=hydrophilic, phob=hydrophobic.

Simulation	Precipitation type	Sulfate	OM phil	OM phob	BC phil	BC Phob	Nitrate	SOA	Sea salt	Dust
CEDSv16/ CMIP6	Convective	1	1	1	1	1	1	0.8	1	1
	LS-liquid	1	1	0	1	0	1	0.8	1	1
	LS-ice	0.1	0.1	0.2	0.1	0.2	0.1	0.16	0.1	0.5
LSIINC	LS-ice	0.3	0.3	0.4	0.3	0.4	0.3	0.32	0.3	0.7
LSIDEC	LS-ice	0.001	0.001	0.1	0.001	0.1	0.001	0.001	0.001	0.1
SOLDEC	Convective	0.8	0.8	0.8	0.8	0.8	0.8	0.6	0.8	0.8
	LS-liquid	0.8	0.8	0	0.8	0	0.8	0.6	0.8	0.8

Table 3: Global, annual mean aerosol burdens [mg m^{-2}] and total AOD in the baseline and sensitivity simulations. Parentheses in the top row give the atmospheric residence time (ratio of burden to total wet plus dry scavenging) [days]. Corresponding values for the sensitivity simulations are given in Table S3.

Simulation	BC	OA	Sulfate	NH4 (fine+coarse)	Nitrate (fine)	Nitrate (coarse)	Sea salt	Dust	AOD
CEDS/CMIP6	0.23 (4.4)	3.4[§] (5.3)	5.4 (5.4)	0.68 (3.5)	0.17 (4.2)	3.9 (5.2)	12 (0.46)	39 (3.4)	0.13
ECLv5	0.21	3.1	5.1	0.65	0.15	3.7	12	39	0.13
RCP/CMIP5	0.18	3.2	5.3	0.63	0.13	3.7	12	39	0.13
LSIINC	0.21	2.8	4.9	0.63	0.17	3.4	11	39	0.12
LSIDEC	0.32	5.3	6.5	0.79	0.16	4.7	14	43	0.16
SOLDEC	0.26	3.6	6.1	0.78	0.16	5.2	15	42	0.15
1x1RES	0.24	3.4	5.6	0.71	0.19	3.6	12	38	0.14
METDTA	0.22	3.0	5.5	0.69	0.16	3.8	12	42	0.13

[§] SOA: 1.1 mg m^{-2} [5.8 days] and POA: 2.3 mg m^{-2} [5.1 days]

Figures

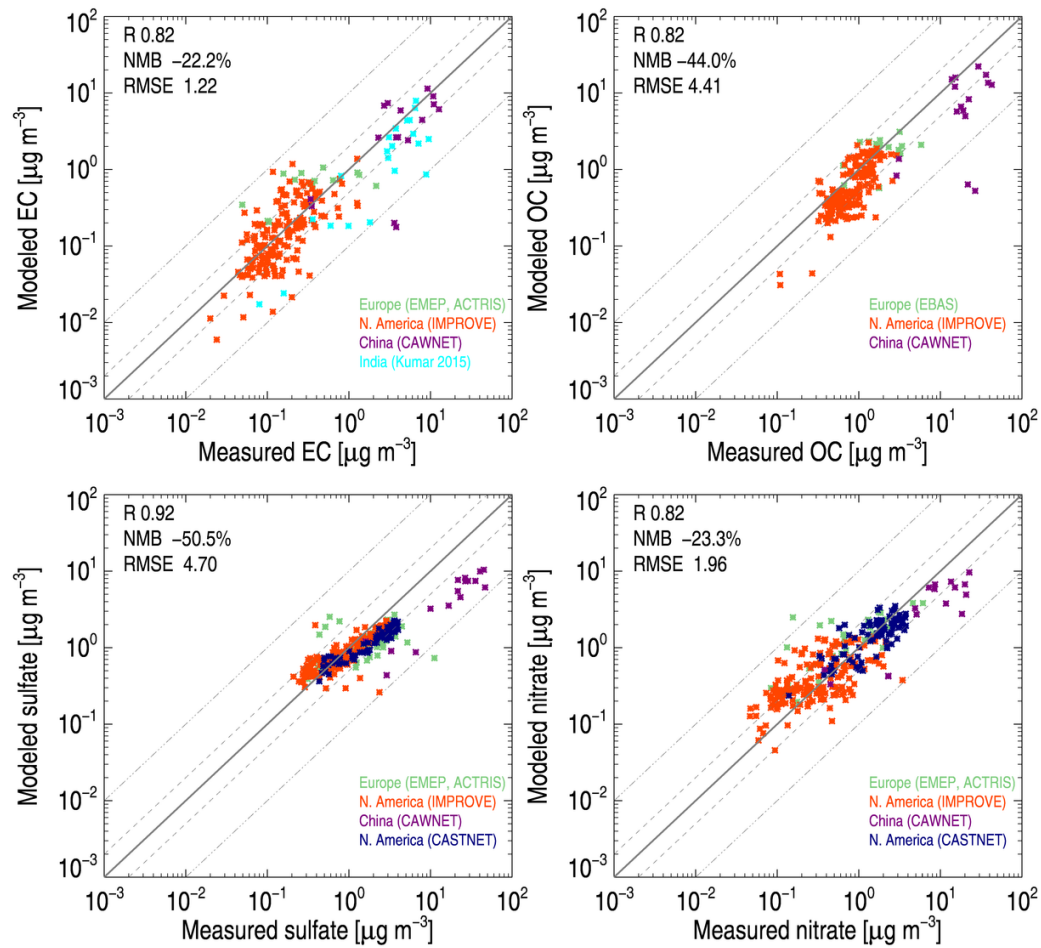


Figure 1: Annual mean modeled versus measured aerosol surface concentrations of a) EC, b)

OC, c) sulfate and d) nitrate from the IMPROVE, EMEP, ACTRIS, CASTNET and CAWNET measurements networks.

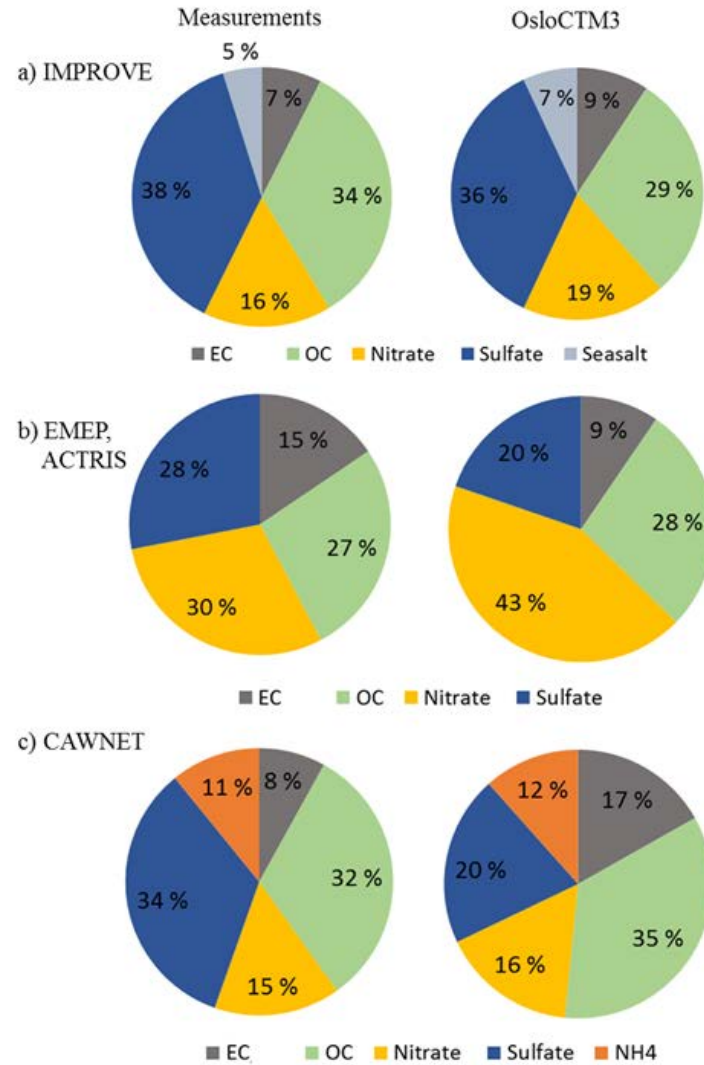


Figure 2: Aerosol composition (fraction of total aerosol mass) derived from the IMPROVE, EMEP, ACTRIS and CAWNET networks (left column) and corresponding OsloCTM3 results (right column).

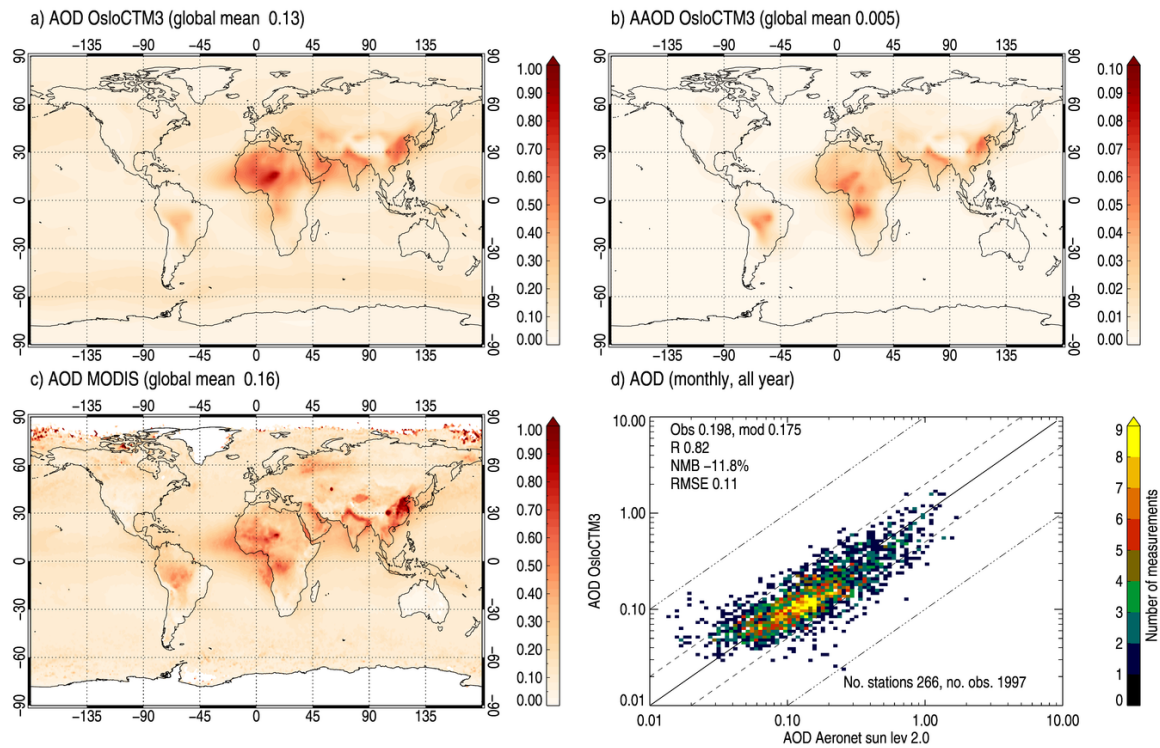


Figure 3: Annual mean (year 2010) modeled a) AOD and b) AAOD, c) MODIS-Aqua AOD retrieval and d) scatter density plot of comparison of simulated AOD against monthly mean AERONET observations.

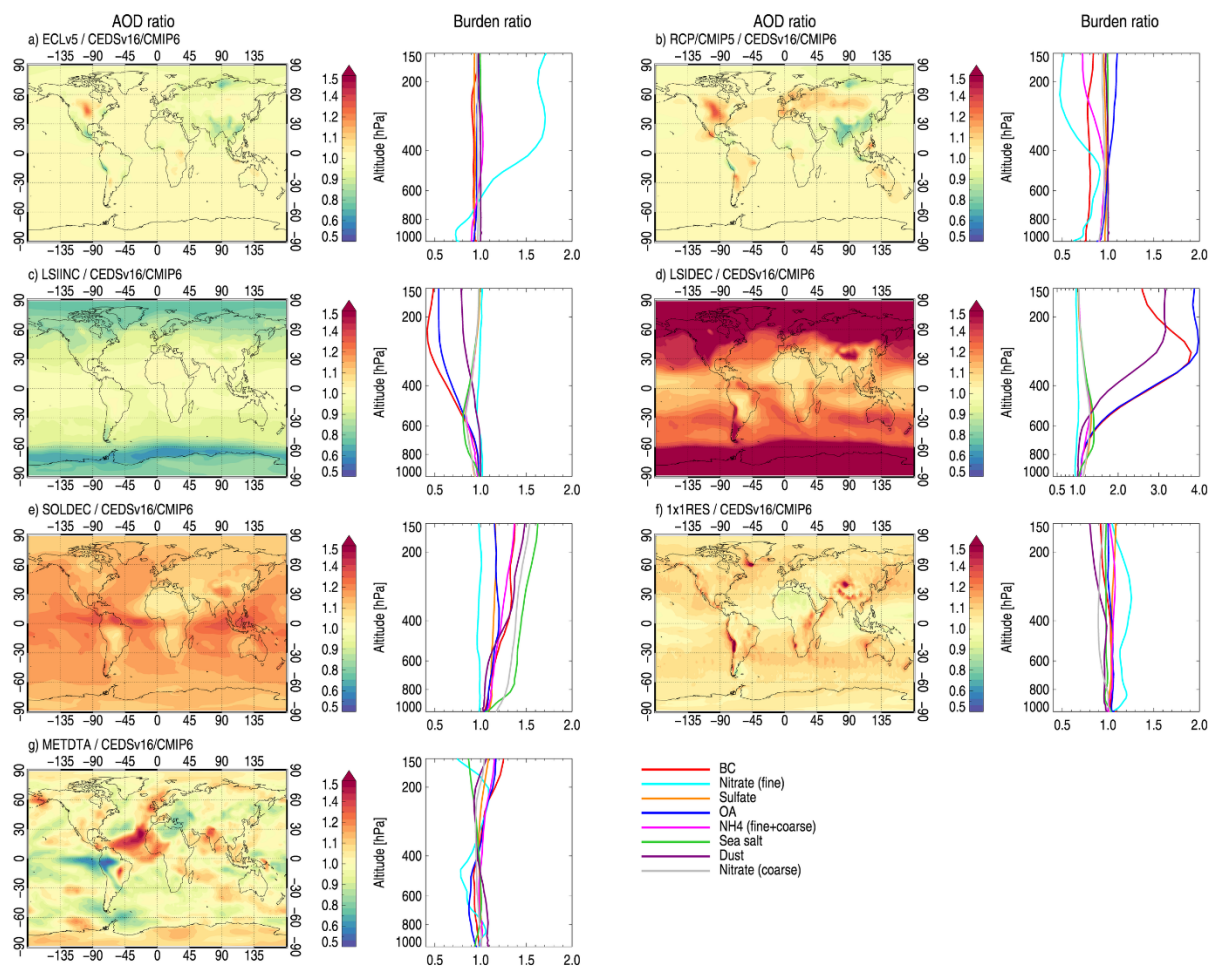
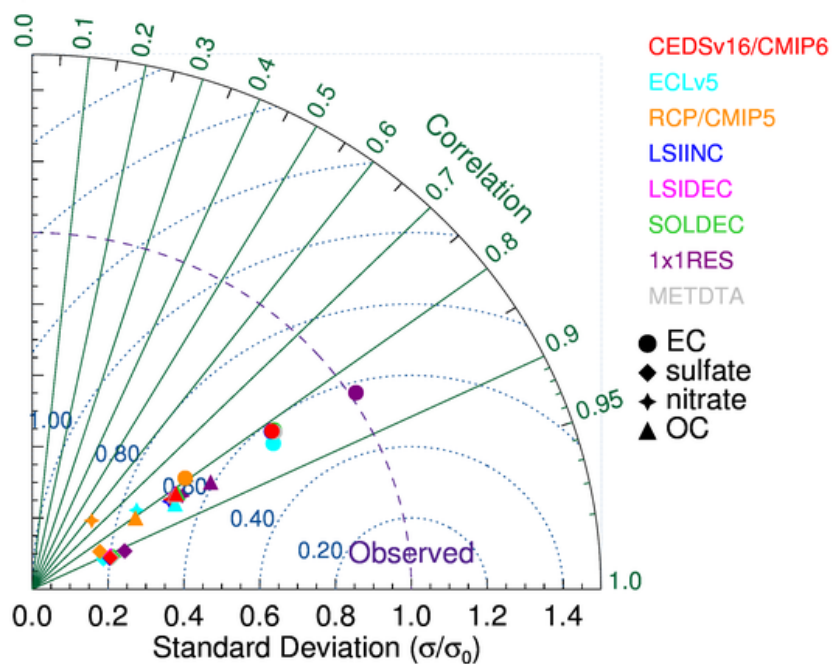


Figure 4: Ratio of each sensitivity simulation relative to the baseline for AOD (columns 1 and 3) and total burden by species in each model layer (columns 2 and 4).

a) Surface concentration



b) AOD

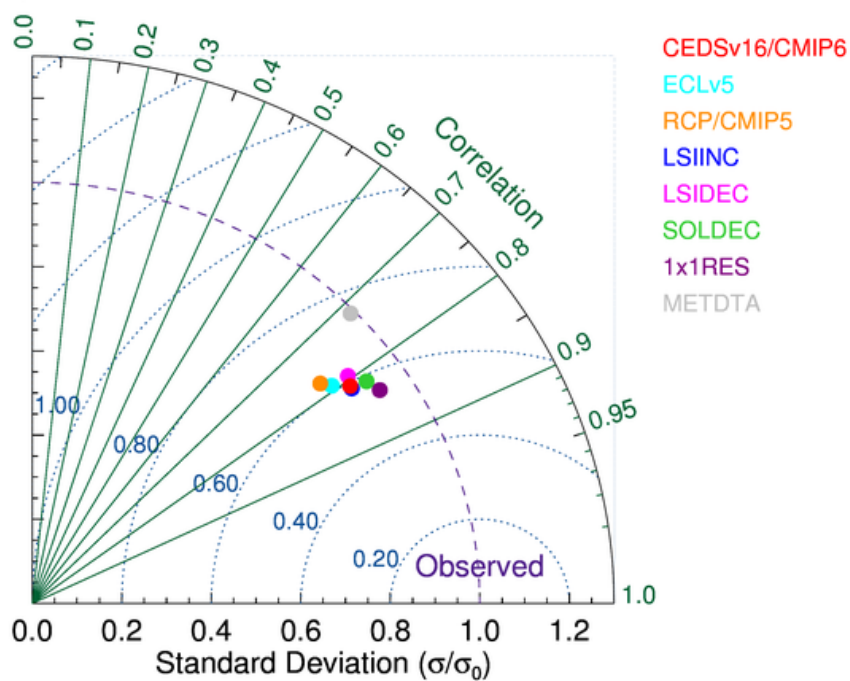
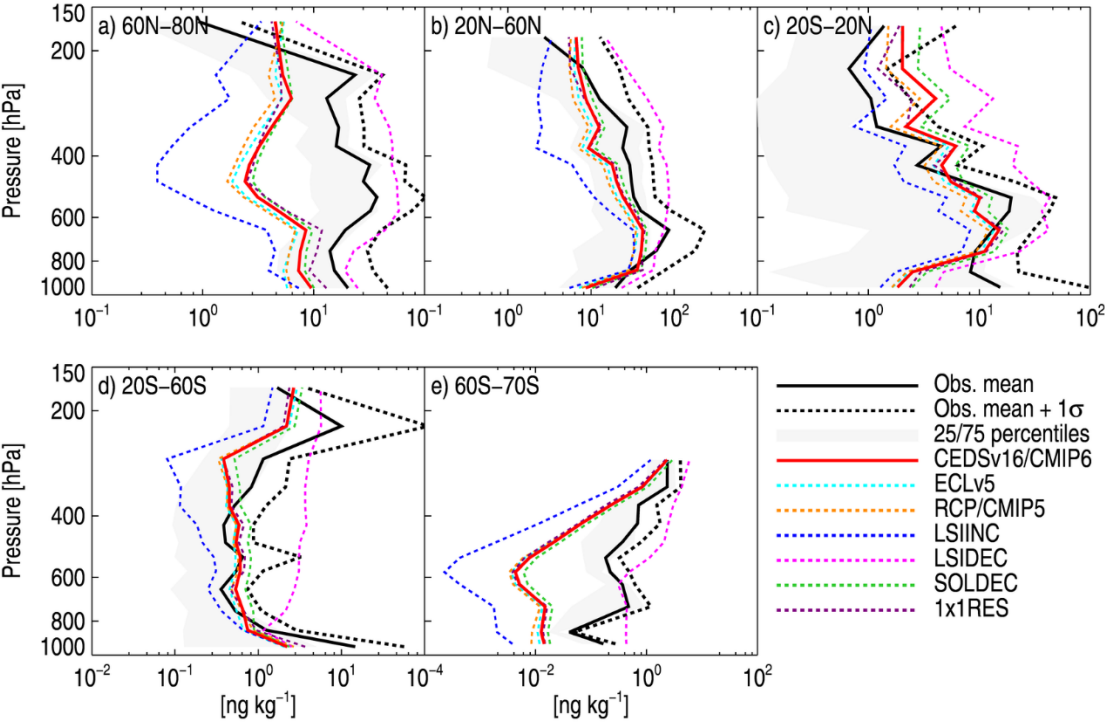


Figure 5: Taylor diagram of modeled and measured aerosol surface concentrations in the baseline simulation and sensitivity tests using all observations in Fig. 1.

1475
1476



1477
1478 *Figure 6: Modeled vertical BC profiles against rBC aircraft measurements in five different*
1479 *latitudes bands over the Pacific Ocean from the HIPPO3 flight campaign. Model data is*
1480 *extracted along the flight track using an online flight simulator. Black lines: mean of*
1481 *observations (solid), mean + plus 1 standard deviation (dashed). Colored lines: OsloCTM3*
1482 *baseline (CEDSv16/CMIP6) (solid), sensitivity simulations (dashed).*

1483
1484
1485

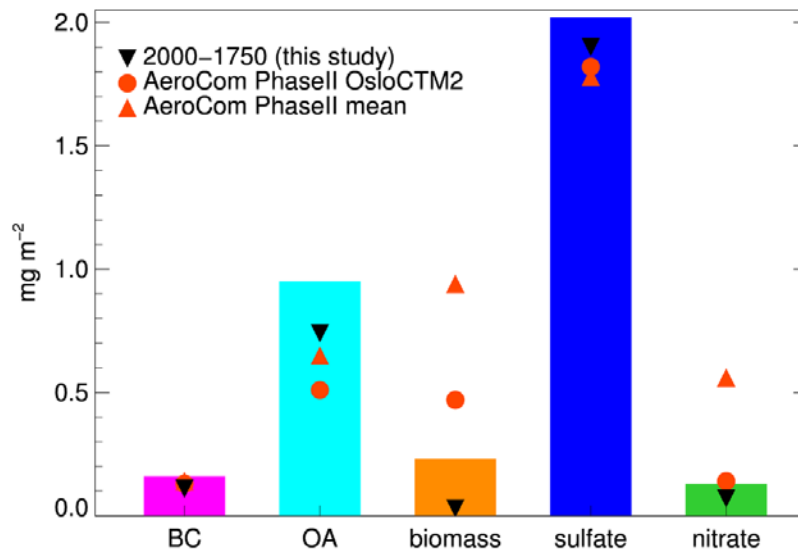


Figure 7: Change in anthropogenic aerosol load over the period 1750 to 2014 using CEDSv16 emissions. Black symbols show the 1750 to 2000 difference and red symbols show multi-model mean and OsloCTM2 results from the AeroCom II experiments [Myhre et al., 2013a].

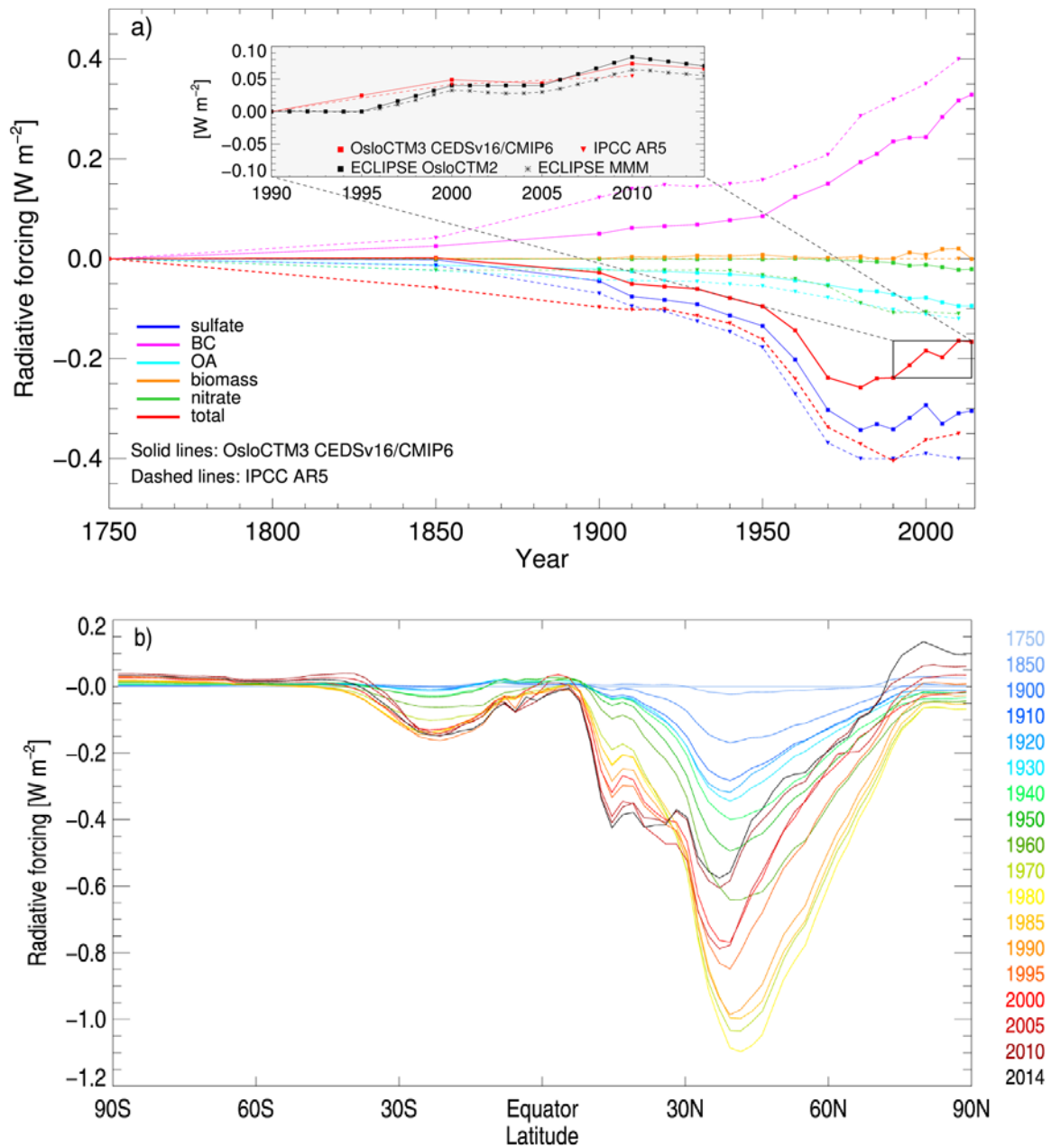


Figure 8: a) Time evolution of RF_{ari} . Solid lines show OsloCTM3 results from the current study, while dashed lines show results from IPCC AR5[Myhre et al., 2013b]. The inset shows the change in total RF_{ari} between 1990 and 2015 in the current study compared with IPCC AR5 and multi-model mean and OsloCTM2 results from Myhre et al. [2017] using ECLv5 emissions. b) zonal mean RF_{ari} 1750-2014.